Acidity and nucleophilic reactivity of glutathione persulfide

Received for publication, June 6, 2020, and in revised form, August 17, 2020 Published, Papers in Press, September 1, 2020, DOI 10.1074/jbc.RA120.014728

Dayana Benchoam[1,2,‡], Jonathan A. Semelak[3,‡], Ernesto Cuevasanta[1,2,4], Mauricio Mastrogiovanni[2,5], Juan S. Grassano[3], Gerardo Ferrer-Sueta[2,6], Ari Zeida[2,5], Madia Trujillo[2,5], Matías N. Möller[2,6,*], Darío A. Estrin[3,*], and Beatriz Alvarez[1,2,*]

From the [1]Laboratorio de Enzimología, Instituto de Química Biológica, Facultad de Ciencias, and [2]Centro de Investigaciones Biomédicas (CEINBIO), Universidad de la República, Montevideo, Uruguay, [3]Departamento de Química Inorgánica, Analítica y Química Física, Instituto de Química Física de los Materiales, Medio Ambiente y Energía (INQUIMAE), Facultad de Ciencias Exactas y Naturales, Universidad de Buenos Aires and CONICET, Argentina, [4]Unidad de Bioquímica Analítica, Centro de Investigaciones Nucleares, Facultad de Ciencias, [5]Departamento de Bioquímica, Facultad de Medicina, and [6]Laboratorio de Fisicoquímica Biológica, Instituto de Química Biológica, Facultad de Ciencias, Universidad de la República, Montevideo, Uruguay

Edited by F. Peter Guengerich

Persulfides (RSSH/RSS$^-$) participate in sulfur trafficking and metabolic processes, and are proposed to mediate the signaling effects of hydrogen sulfide (H_2S). Despite their growing relevance, their chemical properties are poorly understood. Herein, we studied experimentally and computationally the formation, acidity, and nucleophilicity of glutathione persulfide (GSSH/GSS$^-$), the derivative of the abundant cellular thiol glutathione (GSH). We characterized the kinetics and equilibrium of GSSH formation from glutathione disulfide and H_2S. A pK_a of 5.45 for GSSH was determined, which is 3.49 units below that of GSH. The reactions of GSSH with the physiologically relevant electrophiles peroxynitrite and hydrogen peroxide, and with the probe monobromobimane, were studied and compared with those of thiols. These reactions occurred through S_N2 mechanisms. At neutral pH, GSSH reacted faster than GSH because of increased availability of the anion and, depending on the electrophile, increased reactivity. In addition, GSS$^-$ presented higher nucleophilicity with respect to a thiolate with similar basicity. This can be interpreted in terms of the so-called α effect, *i.e.* the increased reactivity of a nucleophile when the atom adjacent to the nucleophilic atom has high electron density. The magnitude of the α effect correlated with the Brønsted nucleophilic factor, β_{nuc}, for the reactions with thiolates and with the ability of the leaving group. Our study constitutes the first determination of the pK_a of a biological persulfide and the first examination of the α effect in sulfur nucleophiles, and sheds light on the chemical basis of the biological properties of persulfides.

Persulfides (RSSH/RSS$^-$)[7] can be formed in biological systems through several pathways, some of which are dependent on hydrogen sulfide (H_2S/HS$^-$)[8]. Beyond its toxicity, H_2S exerts physiological effects with potential health benefits in mammals. Persulfides have been proposed to transduce these effects; the modification of critical protein thiols (RSH/RS$^-$) to persulfides would unleash downstream effects of H_2S (1). In addition, persulfides are intermediates in the biosynthesis of iron-sulfur clusters and other cofactors (2). They also constitute intermediates in the mitochondrial oxidation of H_2S (1).

Persulfides can be formed *in vivo* via reactions of H_2S with oxidized thiol derivatives, *i.e.* disulfides (RSSR′) or sulfenic acids (RSOH) (3), via reactions of thiolates with oxidized sulfur derivatives, *e.g.* polysulfides (HS_nS^-, $n \geq 1$) (4), and via free radical–mediated processes (5). Note that H_2S and thiols do not react directly with each other. H_2S-independent pathways for persulfide synthesis also exist, in which the sulfur is donated by thiols or disulfides (6–9). Moreover, there are enzymes capable of producing, transferring, and reacting with persulfides. Sulfide quinone oxidoreductase (SQOR) catalyzes the oxidation of H_2S to glutathione persulfide (GSSH), the persulfide derivative of the very abundant cellular thiol glutathione (GSH), and reduces ubiquinone (10–12). GSSH is the substrate of persulfide dioxygenase (also called ETHE1) (10, 13), an enzyme that oxidizes GSSH to sulfite (SO_3^{2-}) at the expense of O_2 and whose inborn errors are associated with severe clinical conditions (14). Rhodanese can catalyze the reversible reaction between GSSH and sulfite to form GSH and thiosulfate (10, 12, 15). These processes suggest that GSSH plays key roles *in vivo*; indeed, concentrations of ~35 pmol/mg protein (~7 μM) in mouse liver tissue have been recently reported (16). Despite the growing interest in persulfides, their chemical characteristics are poorly understood.

Hydropersulfides (RSSH) ionize in water to form deprotonated persulfides (RSS$^-$). Compared with thiols, a higher acidity is expected for persulfides (1). In fact, the pK_a of 2-[(3-aminopropyl)amino]ethane persulfide was estimated to be 6.2 ± 0.1, which is lower than the pK_a of 7.6 ± 0.1 determined for the corresponding thiol (17). The pK_a of cumyl persulfide was proposed to be 7 (18), whereas the pK_a of cumyl thiol is

This article contains supporting information.

‡These authors contributed equally to this work.

*For correspondence: Matías N. Möller, mmoller@fcien.edu.uy; Darío A. Estrin, dario@qi.fcen.uba.ar; Beatriz Alvarez, beatriz.alvarez@fcien.edu.uy

[7]The term "persulfide" is used in this text for the mixture of hydropersulfide (RSSH) and persulfide anion (RSS$^-$) in aqueous solution. The IUPAC recommended names for RSSH are hydridodisulfide, disulfanyl, and dithiohydroperoxide.

[8]The term "H_2S" is used in this text for the mixture of hydrogen sulfide (H_2S) and hydrosulfide anion (HS$^-$) in aqueous solution. The IUPAC recommended names are sulfane or dihydrogen sulfide for H_2S, and sulfanide or hydrogen(sulfide)(1–) for HS$^-$.

likely to be higher than 10 according to the values for similar thiols (19). The pK_a of cysteine persulfide was computationally estimated to be ~4 units lower than that of the cysteine thiol (3).

In contrast to thiols, which possess only nucleophilic character, persulfides also have electrophilic character when protonated. The electrophilicity can be ascribed to both sulfur atoms. If the outer sulfur is attacked by a thiolate, the sulfur is transferred and a new persulfide is formed, constituting a transpersulfidation reaction. If the inner sulfur is attacked, H_2S is released and a mixed disulfide is formed.

Persulfides have been proposed to be stronger nucleophiles than thiolates. Enhanced reactivities were observed for arylpersulfides compared with arylthiolates toward alkyl halides in organic solvent (20). Enhanced reactivities were also observed for the persulfides formed in albumin and in the *Mycobacterium tuberculosis* peroxiredoxin AhpE toward 4,4′-dithiodipyridine compared with the corresponding protein thiols (3, 21). In addition, under certain conditions, GSSH reacted with H_2O_2 whereas GSH did not (7), and persulfide reactions with one-electron oxidants were faster than those of thiols (18, 22). The high nucleophilicity of persulfides can be understood in terms of the so-called α effect (3, 20, 23, 24). The α effect was first defined as the enhancement of nucleophilicity when the atom adjacent to a nucleophile bears a lone pair of electrons (25). This definition is ambiguous because the α nucleophile can be compared either with a structural analog (*e.g.* HOO^- and HO^-, NH_2-NH_2 and NH_3, and RSS^- and RS^-) or with a nucleophile of equal basicity, in the context that for several reactions nucleophilicity correlates with Brønsted basicity. Given that the α nucleophile is not always more reactive than the structural analog (26), the α effect is more accurately defined as the positive deviation from the corresponding Brønsted plot (log *k versus* nucleophile pK_a) (27, 28). For this definition to be valid, the α and reference nucleophiles should react by similar mechanisms (29).

Because of their dual nucleophilic and electrophilic character, persulfides decay in aqueous solution, making their preparation and quantification challenging. Many methods for persulfide determination are either indirect, slow, or unspecific (1). The direct detection by MS is inconvenient because of their instability. Thus, derivatization with different alkylating agents, *e.g.* iodoacetamide, *N*-ethylmaleimide, or monobromobimane (mBrB) (7, 23, 30, 31), has become a common practice in which the rate of the alkylation step is crucial (30).

The reaction between glutathione disulfide (GSSG) and H_2S forms GSSH and GSH in a reversible process (3, 23, 32). This reaction is often used to prepare GSSH *in vitro* (13, 23, 31), and sometimes the concentration of the formed GSSH is estimated from that of the produced GSH or from the initial reactants, assuming stoichiometric relations. Nevertheless, because of the reactivity of persulfides, subsequent reactions are likely to happen and affect the yield, calling for a better characterization of the mixtures.

Considering that persulfides are involved in biosynthesis and catabolism, and that they play roles in cellular signaling, it is important to better understand their chemical properties. Herein, we studied the formation, acidity, and nucleophilicity of GSSH. A method to quantify GSSH was adapted and subsequently employed to characterize the reaction between GSSG and H_2S, providing kinetic and equilibrium constants. The pK_a of GSSH was determined, representing the first pK_a report for a persulfide formed in biological systems. The nucleophilicity of GSSH toward mBrB, peroxynitrite ($ONOOH/ONOO^-$)[9], and H_2O_2 was investigated. These electrophiles were chosen because there is information available for their reactions with thiols, enabling comparison. In addition, mBrB facilitates monitoring of the reactions by fluorescence, whereas peroxynitrite and H_2O_2 are biologically relevant oxidants. To understand the molecular basis of the differential reactivity, we performed hybrid quantum-classical (quantum mechanics/molecular mechanics, QM/MM) calculations for the model pair methanethiolate/methanepersulfide anion ($MeS^-/MeSS^-$) toward the same electrophiles. Our results provide the first quantitative study of the nucleophilicity of a persulfide and its comparison with thiols. This constitutes, to our knowledge, the first examination of the α effect in sulfur nucleophiles.

Results and discussion

Quantification of GSSH

A reversed-phase HPLC method based on mBrB derivatization (7, 33–35) was adapted to quantify GSSH in a mixture of species. GSSG and H_2S reacted to form GSH and GSSH, and excess mBrB was added to label H_2S, GSH, and GSSH as the derivatized species B-S-B, GS-B, and GSS-B, respectively (Fig. 1*A*). A peak with a retention time of 7.7 min was ascribed to GSS-B because it disappeared in the presence of the reductant tris(2-carboxyethyl)phosphine (TCEP), and when more mBrB was added, GS-B and B-S-B increased. The peaks corresponding to GSSG, GS-B, and B-S-B were assigned using standards (retention times of 5.8, 7.3, and 9.8 min, respectively) (Fig. 1*B*). The identities of the four species were confirmed by electrospray ionization MS and MS/MS; the results for GS-B and GSS-B were consistent with a mass increase of 32 Da for the latter (Fig. 1*C*). Calibration curves at 260 nm for GSSG and at 396 nm for GS-B and B-S-B were performed. Considering that GSS-B and GS-B have the same absorptivity at 396 nm because of the bimane moiety, the calibration curve for GS-B was used to quantify GSS-B.

To measure accurate concentrations, the derivatization step must be faster than the interconversion of species (30). Because reaction rates are the products of rate constants and concentrations, it can be calculated that labeling was ≥100-fold faster than interconversion in our conditions (3, 30, 35–38). Indeed, the detected concentrations of GSH and GSSH were independent of the amount of mBrB applied (Fig. S1). Furthermore, GSS-B was relatively stable and its decay within 100 min was minor (Fig. S2). In summary, under the conditions employed herein, the concentration of the derivatives represent those present in the original mixtures.

[9] The term "peroxynitrite" is used in this text for the sum of peroxynitrous acid (ONOOH) and peroxynitrite anion ($ONOO^-$). The IUPAC recommended names are hydrogen oxoperoxonitrate and oxoperoxonitrate (1−), respectively.

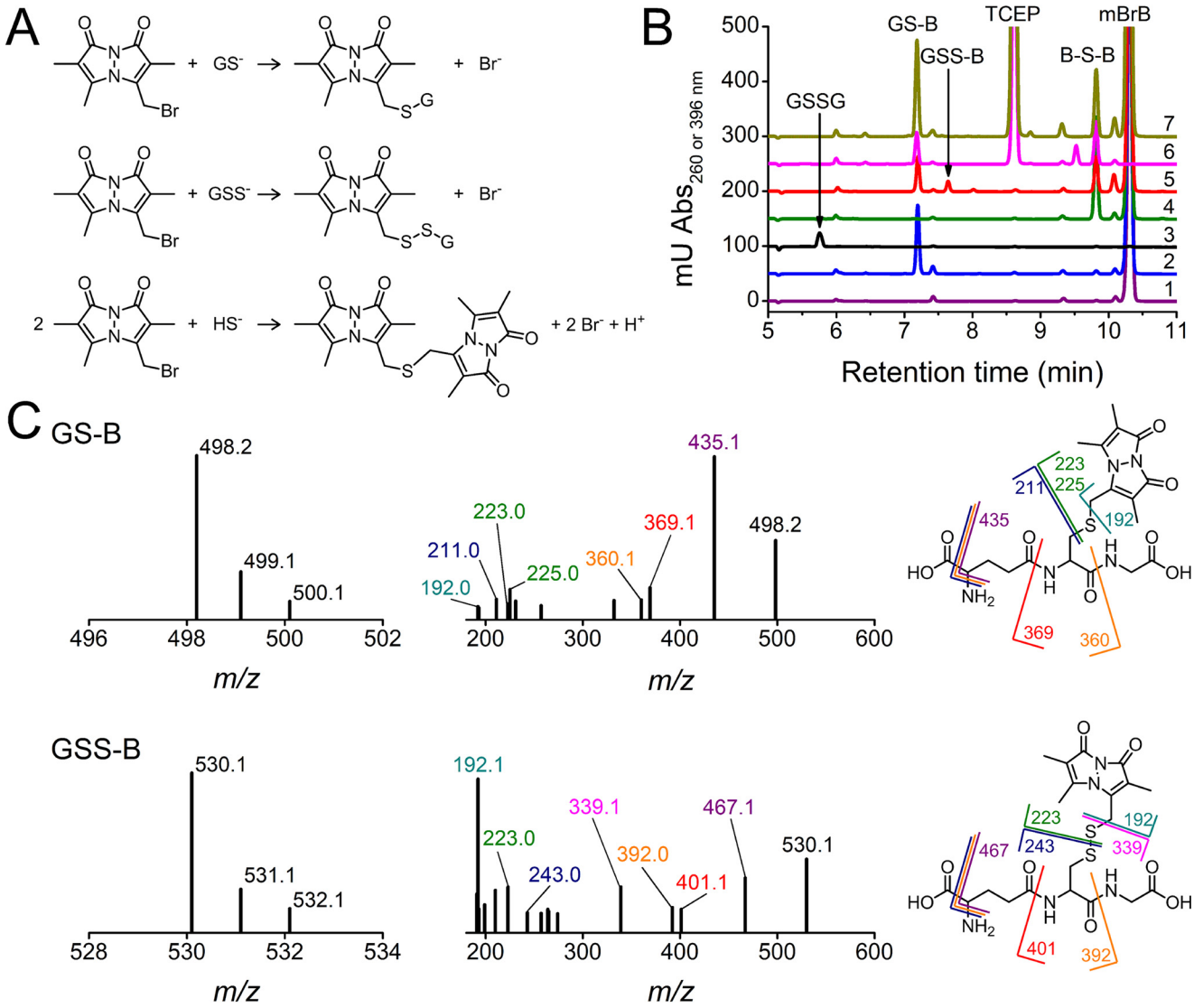

Figure 1. Derivatization with mBrB and characterization of chromatographic peaks. *A*, reactions of GSH, GSSH, and H_2S with mBrB to form GS-B, GSS-B, and B-S-B, respectively. *B*, representative HPLC runs of 1) mBrB (2 mM), 2) GS-B (0.2 mM), 3) GSSG (1 mM), 4) B-S-B (0.2 mM), 5) mixture of GSSG and H_2S (3 mM each, 20 min) diluted 15-fold and incubated with mBrB (2 mM), 6) reduction of 5 with TCEP (4.5 mM), and 7) addition of mBrB (6.9 mM) to 6. Reactions were done in phosphate buffer (0.1 M, pH 7.4, 25 °C). All chromatograms were recorded at 396 nm, except 3 (GSSG) at 260 nm. *C*, mass spectra and fragmentation patterns of the fractions eluting at 7.3 (GS-B, *m/z* 498.2) and 7.7 min (GSS-B, *m/z* 530.1). The product ions of GS-B are ascribable to neutral loss of NH_3 and HCOOH (435.1), minus glycine (360.1), or minus a sulfur-bimane derivative (211.0), loss of glutamate (369.1), and formation of the sulfur-bimane derivative (223.0 and 225.0). The fragmentation pattern of GSS-B showed peaks analogous to GS-B plus 32 (sulfur atom), assigned to the loss of NH_3 and HCOOH (467.1), minus glycine (392.0), or minus the sulfur-bimane derivative (243.0), loss of glutamate (401.1), and the formation of the sulfur-bimane derivative (223.0). The peak at *m/z* 339.1 could correspond to the protonated homolysis product GSS$^{\bullet}$. Fragments of *m/z* 192 were assigned to the bimane protonated radical as previously observed (7, 30, 36).

Kinetics and thermodynamics of the reaction of GSSG with H_2S

Given the feasibility of quantifying GSSG, GSH, GSSH, and H_2S, we first studied the kinetics of the reaction of GSSG and H_2S (Reaction 1).

$$\mathrm{GSSG} + \mathrm{H_2S} \underset{k_{-1}}{\overset{k_1}{\rightleftharpoons}} \mathrm{GSH} + \mathrm{GSSH}$$

Reaction 1

GSSG (5–11 mM) was incubated with H_2S (0.5 mM), and the reactions were stopped at different times by dilution and derivatization with mBrB. Time courses were obtained, and a second-order forward rate constant ($k_{1,pH}$) of 0.23 ± 0.02 M^{-1} s^{-1} (pH 7.46, 24 °C) was determined from H_2S decay (Fig. 2, *A* and *B*). This is in agreement with the reported value of 0.16 ± 0.01 M^{-1} s^{-1} (pH 7.4, 25 °C) previously determined by the methylene blue method (3).

The final concentration of GSSH was always lower than that of GSH. Furthermore, the final concentration of GSSH was lower than the initial concentration of H_2S (the limiting reagent) whereas that of GSH was higher (Fig. 2*A*). Considering that GSSG was in excess, it is proposed that GSSH and GSSG reacted in a second relatively fast reaction to form glutathione trisulfide (GSSSG) and GSH (Reaction 2).

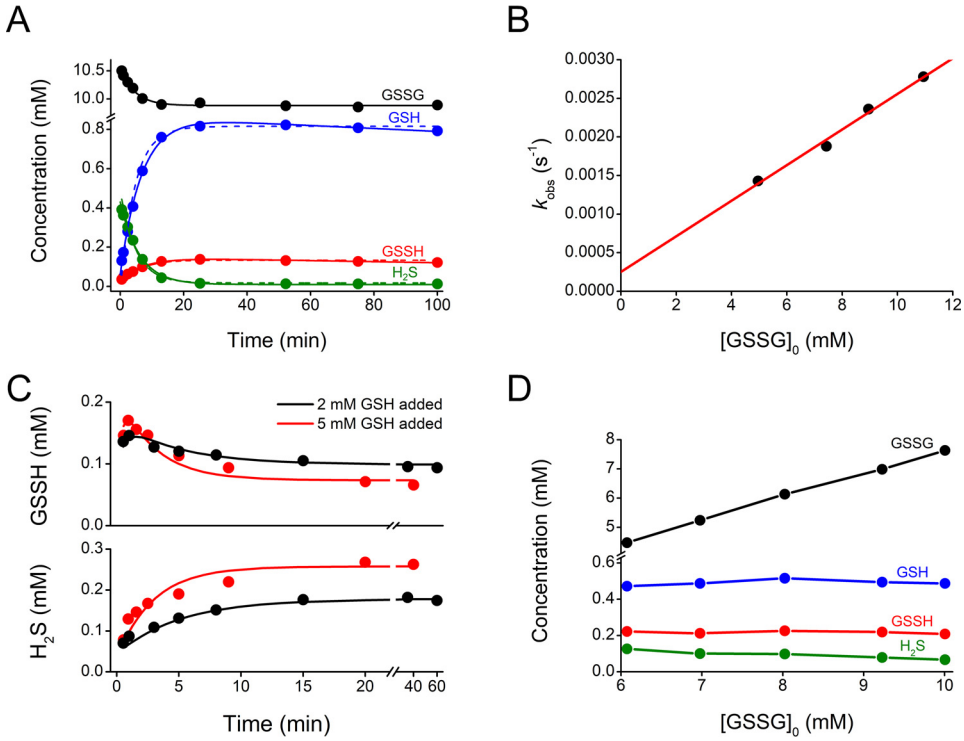

Figure 2. Kinetics and thermodynamics of the reaction of GSSG and H_2S to give GSH and GSSH. *A*, time courses of the reaction between GSSG (11 mM) and H_2S (0.5 mM) in phosphate buffer (0.1 M, pH 7.4, 25 ± 1 °C). *Solid lines* represent the fitted single exponential or exponential plus linear functions. The rate constants of a model consisting of Reactions 1 and 2 were estimated with COPASI using four independent experiments, obtaining $k_{1,pH}$ = 0.33 ± 0.01, $k_{-1,pH}$ = 0.51 ± 0.08, $k_{2,pH}$ = 1.6 ± 0.3, and $k_{-2,pH}$ = 9 ± 2 M^{-1} s^{-1}. *Dashed lines* represent simulated time courses for a representative experiment. *B*, exponential rate constants (k_{obs}) of H_2S decay *versus* initial GSSG. The $k_{1,pH}$ obtained from the fit of four independent experiments was 0.23 ± 0.02 M^{-1} s^{-1} (pH 7.46 ± 0.01, 24 °C). *C*, mixtures of GSSG (5 mM) and H_2S (0.5 mM), preincubated for 1 h in the mentioned buffer, were exposed to 2–12.5 mM GSH, and the reactions were followed by derivatization and HPLC (pH 7.28 ± 0.05, 25 °C). Using eight independent experiments, COPASI simulations in which $k_{1,pH}$ was fixed to 0.23 M^{-1} s^{-1}, and initial concentrations of GSSG, GSSH, and H_2S were 3.7 mM, 90 μM, and 50 μM, respectively, according to HPLC quantification, yielded $k_{-1,pH}$ = 1.11 ± 0.06, $k_{2,pH}$ = 2.3 ± 0.5, $k_{-2,pH}$ = 3.1 ± 0.4 M^{-1} s^{-1}, and $[GSSSG]_0$ = 0.27 ± 0.01 mM. *Solid lines* represent simulated time courses for two representative experiments. *D*, equilibrium concentrations. GSSG (6–10 mM) and H_2S (0.5 mM) were incubated in the mentioned buffer under shaking. After 2 h, 4 mM mBrB was added and the GSSH-containing mixtures were analyzed by HPLC. The apparent equilibrium constant of Reaction 1 obtained from six independent determinations was 0.194 ± 0.005 (mean ± S.D., pH 7.4, 25 °C.).

$$\mathrm{GSSH} + \mathrm{GSSG} \underset{k_{-2}}{\overset{k_2}{\rightleftharpoons}} \mathrm{GSH} + \mathrm{GSSSG}$$

Reaction 2

Accordingly, MS analysis of a mixture of excess GSSG and H_2S derivatized with iodoacetamide presented a peak with a *m/z* of 645.1, consistent with GSSSG (not shown). This is in agreement with previous reports where the corresponding trisulfides were observed (30, 39). The low sensitivity at 260 nm might have precluded the chromatographic detection of GSSSG. In addition, GSSSG was unlikely to co-elute with the characterized species, because it was not detected in the mass spectra of the chromatogram peaks but appeared in the mass spectrum of the whole mixture.

Rate constants were estimated with the software COPASI (40) using a model consisting of Reactions 1 and 2 and four independent sets of time courses of GSSH, GSH, and H_2S. Values of $k_{1,pH}$ = 0.33 ± 0.01, $k_{-1,pH}$ = 0.51 ± 0.08, $k_{2,pH}$ = 1.6 ± 0.3, and $k_{-2,pH}$ = 9 ± 2 M^{-1} s^{-1} were obtained (Fig. 2*A*). The value of $k_{1,pH}$ was consistent with that obtained from H_2S decay (0.23 M^{-1} s^{-1}, Fig. 2*B*).

Regarding the physiological relevance of the reaction between GSSG and H_2S, and considering the relatively low rate constant (0.23 M^{-1} s^{-1}) and concentration of GSSG *in vivo* (<5 μM in cytosol of yeast (41, 42)), it can be concluded that GSSG is unlikely to constitute a major consumer of H_2S compared with preferential targets. Among the preferential targets of H_2S, SQOR deserves special mention because, in addition to reacting very fast with H_2S ($k_{cat}/K_{m,H2S}$ = 1.1 × 10^7 M^{-1} s^{-1}, pH 7.4), it can form GSSH as product (11, 12).

To obtain a better estimate of the kinetics of the reverse Reaction 1, GSH (2–12.5 mM) was added to a mixture of GSSG and H_2S (pH 7.28, 25 °C) that had been preincubated for 1 h. At consecutive times, aliquots were analyzed. GSSH time courses showed a fast increase followed by a slower decrease, whereas H_2S increased (Fig. 2*C*). This is consistent with Reactions 1 and 2, whereby GSSH is rapidly formed by GSH and GSSSG (reverse Reaction 2) and consumed by GSH forming H_2S and GSSG in a slower process (reverse Reaction 1). Because both reactions are reversible, GSSH was not completely consumed. Eight independent time courses of GSSH and H_2S were analyzed with COPASI (40) according to a model consisting of Reactions 1 and 2, yielding $k_{-1,pH}$ = 1.11 ± 0.06, $k_{2,pH}$ = 2.3 ± 0.5, $k_{-2,pH}$ = 3.1 ± 0.4 M^{-1} s^{-1}, and an initial concentration of GSSSG of 0.27 ± 0.01 mM (Fig. 2*C*). This experimental design allows a more robust estimation of $k_{-1,pH}$ than that of Fig. 2*A*. The estimated concentration of GSSSG was consistent with

mass balance considerations that initial H_2S equals the sum of H_2S, GSSH, and GSSSG in equilibrium and with previous observations under conditions of excess GSSG that the concentration of GSSSG is ~1/2 GSH in equilibrium (30). In our case, the concentrations of GSSH inferred from these relationships matched by 93 ± 8% (n = 6) those measured by HPLC. Of note, our kinetic analysis contemplated only two reactions. Whereas this simplification is reasonable when excess GSSG is used, other minor processes may probably occur, *e.g.* reaction of GSS^- with GSSSG or GSSH.

Reactions with thiolates constitute one of the main decay pathways for persulfides *in vivo* (16, 43, 44). To our knowledge, the value of $k_{-1,pH}$ (1.11 M^{-1} s^{-1}) is the first report for the rate constant of a reaction between a low molecular weight (LMW) persulfide and a LMW thiolate at physiological pH. While there is an estimation for cysteine persulfide and cysteine of 0.09 ± 0.01 M^{-1} s^{-1} (45), it corresponds to pH 10, a condition in which the carboxylate and amine of cysteine are deprotonated, likely affecting the kinetics of reaction (46).

We also analyzed the composition of the GSSH-containing mixtures once the concentrations remained stationary. GSSG (6–10 mM) and H_2S (0.5 mM) were incubated for 2 h, the reactions were stopped, and the species were quantified (Fig. 2*D*). A concentration quotient of 0.194 ± 0.005 (pH 7.4, 25 °C, 0.1 M phosphate buffer) was obtained for Reaction 1. Assuming that irreversible processes such as H_2S release, elemental sulfur precipitation, or oxidation by oxygen are insignificant in this timescale, this quotient reflects the apparent equilibrium constant ($K_{eq1,pH}$) of Reaction 1 at pH 7.4. The value is consistent with $k_{1,pH}$ being lower than $k_{-1,pH}$ and with the apparent equilibrium constant calculated from kinetic experiments ($k_{1,pH}/k_{-1,pH}$ = 0.21).

From the apparent $K_{eq1,pH}$ of 0.194, the $\Delta G°'$ of Reaction 1 can be calculated to be +1.0 kcal/mol (pH 7.4, 25 °C). This agrees with a value of +1.4 kcal/mol estimated from thermochemical calculations for a generic RSSR reacting with HS^- to form RSS^- and RSH (the predominant species at neutral pH) (47) and supports that the Gibbs energy change is close to zero at physiological pH.

Our results underscore the existence of reverse and consecutive reactions and, together with the fact that persulfides disproportionate, indicate that GSSH cannot be purified in aqueous solutions; instead, it will be stationarily present in a mixture of species. This assertion is supported by several unsuccessful attempts to purify GSSH (not shown). Our results also lead to a note of caution for situations in which the concentration of persulfides is estimated from the thiol formed or from the initial concentration of reactants, because the quantities formed are not stoichiometric.

Acidity of GSSH and kinetics of the reaction with mBrB

After the GSSH-containing mixture had been characterized, the pK_a of GSSH was measured by the pH dependence of the reaction with mBrB, exploiting that mBrB does not accept or release protons within the pH range studied and that the reactions can be followed by product fluorescence. As previously performed for GSH, an initial rate study was performed (37, 48) by reacting low concentrations of a GSSH-containing mixture and mBrB at different pHs at 25 °C. The initial slopes of the fluorescence variations increased with pH according to a one-pK_a function, yielding a pK_a of 5.50 ± 0.08 (Fig. 3*A*). The contributions of GSH and H_2S to the fluorescence change were calculated from the known rate constants, initial concentrations, and pK_a values, and found to be negligible (*e.g.* 0.015 and 0.007%, respectively, of the contribution of GSSH at pH 6) (30, 35–38).

Furthermore, we studied the pH dependence of the second-order rate constant (k_{pH}) by reacting GSSH-containing mixtures with excess mBrB. The fluorescence increases were biphasic and exponential plus linear functions were fitted. The fast exponential phase was attributed to the reaction of mBrB with GSSH, whereas the slow linear phase was attributed to the reaction with GSH and, secondarily, with H_2S, based on controls and on the rate constants for GSH and H_2S (Fig. 3*B*) (30, 35–38). Moreover, the amplitude was consistent with independent HPLC determinations of GSS-B, assuming similar fluorescence quantum yield as GS-B. Possibilities such as reaction of mBrB with GSS_nS^- or HS_nS^- (n ≥ 1) cannot be discarded for the fast exponential phase. However, given that our mixtures had excess GSSG, the concentration of these species, if formed, is likely to be low. The k_{obs} attributed to GSSH increased linearly with mBrB concentration. The k_{pH} had a sigmoid dependence with pH, resulting in a pK_a of 5.45 ± 0.03 and a pH-independent rate constant (k_{ind}) for the reaction of GSS^- with mBrB of (9.0 ± 0.2) × 10^3 M^{-1} s^{-1} (Fig. 3, *C–E*). The k_{ind} represents the rate constant that would be measured if all the persulfide were ionized and shows that, with mBrB, the persulfide anion reacts 44 times faster than the thiolate of glutathione (208 M^{-1} s^{-1}) (37). At pH 7.4, GSSH reacted with an apparent rate constant of (7.02 ± 0.04) × 10^3 M^{-1} s^{-1}, 1200 times faster than that with GSH (Table 1). Importantly, similar pK_a values were obtained from both the initial rate and integral methods.

To sum up, the pK_a of GSSH was 5.45 ± 0.03, 3.49 units below that of GSH (8.94) (37). This means that at pH 7.4, the availability of the deprotonated species is 2.8% for GSH but 99% for GSSH.

We then performed a computational analysis of the acidity of persulfides and thiols by electronic structure calculations with the aim of understanding the molecular basis of the difference. The ionization equilibrium of an acid XH can be dissected in several steps: XH and H_2O desolvation, homolytic X-H bond cleavage, $X^•$ electron affinity and hydrogen ionization, H_2O proton affinity, and X^- and H_3O^+ solvation. The energetics of each step can be separately computed at different levels of theory. Then, the standard Gibbs energy change for the global process ($\Delta G_a^°$) can be calculated as the sum of the individual steps, and the contribution of each step to the global process can be discerned. Gibbs energy calculations were performed with the simplified models methanepersulfide (MeSSH) or methanethiol (MeSH) to avoid the optimization of zwitterionic structures in vacuum. Although the electronic structure method and basis sets used affected the computed values, general trends were maintained (Table S1).

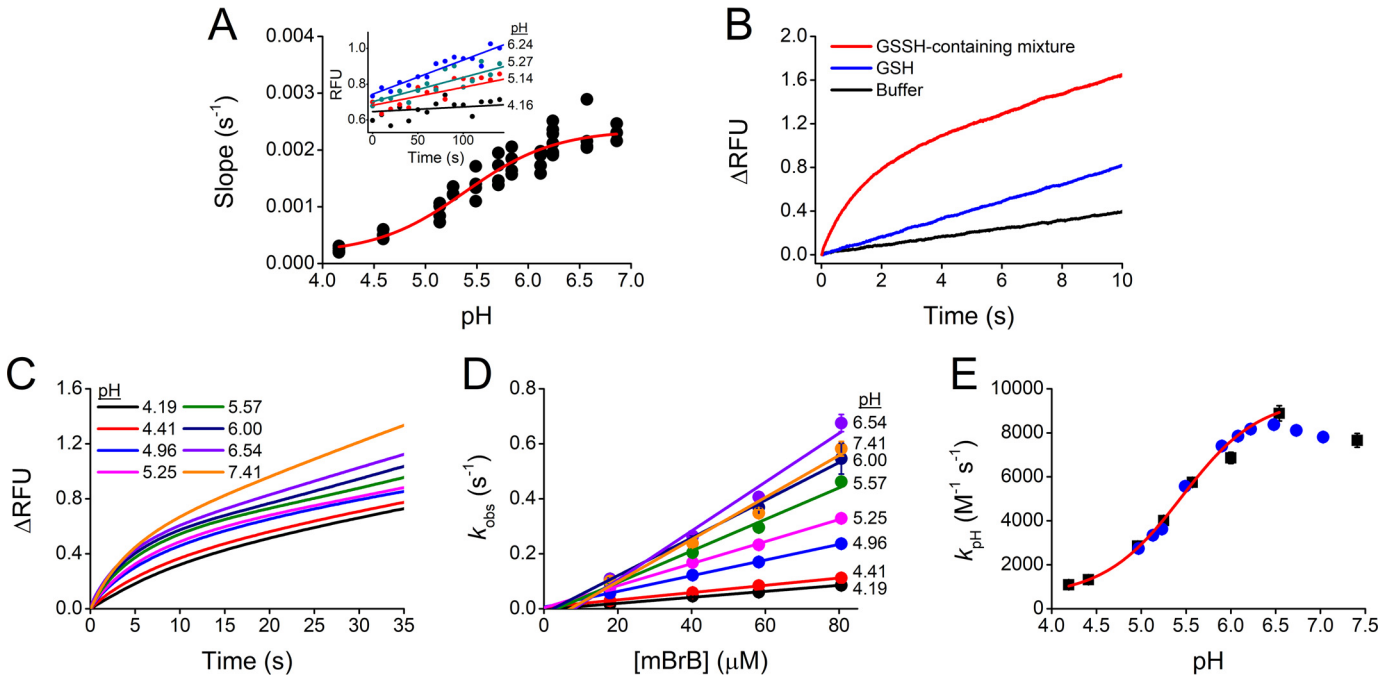

Figure 3. pH dependence of the reaction of GSSH with mBrB. *A*, a mixture containing GSSH (~0.75 μM) reacted with mBrB (1 μM) in acetic/MES/tris buffer (pHs 4.16–6.86, 25 °C). Linear functions fitted to initial fluorescence increases (λ_{ex} = 396 nm, λ_{em} = 472 nm) yielded slopes (*inset*) that had a sigmoid dependence with pH. The data pooled from two independent experiments gave a pK_a of 5.50 ± 0.08 (parameter ± error of the fit). The points shown are quadruplicates of one representative experiment. No interference from the buffer was detected. *B*, representative stopped-flow fluorescence kinetic traces (λ_{ex} = 396 nm, emission cutoff 435 nm) of the reaction of 118 μM mBrB with a mixture containing ~1.6 μM GSSH, ~6.3 μM GSH, and ~1 μM H_2S (final concentrations) in phosphate buffer (0.1 M, pH 7.40, 25 °C, 0.1 mM dtpa) (*red*) and with controls of 6.3 μM GSH (*blue*) or buffer alone (*black*). *C*, GSSH-containing mixtures (~2 μM GSSH) reacted with 18–81 μM mBrB in acetic/MES/Tris buffer (pHs 4.19–7.41, 25 °C). Representative stopped-flow fluorescence time courses with 40 μM mBrB. Exponential plus linear or double exponential plus linear functions were fitted to kinetic traces during 10 half-lives. At the more acidic pHs, an additional fast phase was noted; the origin is unclear but its amplitude was less than 15% of the sum of the amplitudes and was not studied further. *D*, k_{obs} attributed to the reaction of GSSH against mBrB concentration. The *circles* represent the mean ± S.D. of repetitions of a representative experiment. *Error bars* are usually smaller than symbols. The slopes of the fits represent the second-order rate constants. At the more alkaline pHs, a small negative *y*-intercept was observed, probably because of reactant impurities or to a fast reaction with a species present in low concentration. *E*, second-order rate constants *versus* pH. A one-pK_a function fitted the data pooled from two independent experiments (*black squares* and *blue circles*), giving a pK_a of 5.45 ± 0.03 and a maximum (pH-independent) second-order rate constant of (9.0 ± 0.2) × 10^3 M^{-1} s^{-1} (parameters ± errors of the fit). A small but systematic decrease in the k_{pH} at pH > 6.5 was observed, and its cause is unknown.

Table 1
Rate constants for the reactions of GSSH with electrophiles and comparison with those of thiols

	k_{pH}^{GSSH} (M^{-1} s^{-1})	k_{ind}^{GSSH} (M^{-1} s^{-1})	$\frac{k_{pH}^{GSSH}}{k_{pH}^{GSH}{}^{a}}$	$\frac{k_{ind}^{GSSH}}{k_{ind}^{GSH}{}^{a}}$	$\frac{k_{ind}^{GSSH}}{k_{ind}^{RSH\ pK_a\ 5.45}}$	β_{nuc} for the reaction with LMW thiolates
mBrB	(7.02 ± 0.04) × 10^{3}[b]	(9.0 ± 0.2) × 10^3	1200[b]	44	1670	0.52 ± 0.08
Peroxynitrite	(1.25 ± 0.03) × 10^{5}[c]	(4.7 ± 0.1) × 10^5	97[c]	1.8	50	0.42 ± 0.06[d]
H_2O_2	7.5 ± 0.6[e]	7.7 ± 0.6	22[e]	0.24	3.2	0.27 ± 0.06

[a]Reported rate constants for the reactions of GSH with mBrB (37), peroxynitrite (54, 56), and H_2O_2 (37).
[b]Rate constants at pH 7.40, 25 °C.
[c]Rate constants at pH 7.23, 37 °C.
[d]β_{nuc} calculated in this paper (see legend to Fig. 6).
[e]Rate constants at pH 7.02, 25 °C.

The thermodynamic relation between the Gibbs energy change and the acidity constant is given by Equation 1, where R is the ideal gas constant and T is the temperature.

$$\Delta G_a^{\circ} = 2.303\,RT\,pK_a \qquad \text{(Eq. 1)}$$

A difference in pK_a between thiol and persulfide (ΔpK_a) of 7.2 was calculated using Equation 1 and Gibbs energy changes obtained for the global ionization process with the electronic structure coupled cluster singles and doubles method (CCSD) employing the 6-31 G(d′) basis set. However, small errors (~1 kcal/mol) in the computed Gibbs energies would affect the estimated pK_a values. The main difference in the energetics of the individual steps between thiol and persulfide was found in the homolytic S-H bond cleavage, which was ~20% lower for MeSSH than for MeSH (Table S1). This is consistent with S-H bond dissociation energies reported for alkyl thiols and persulfides, which differed by 24% (49), and with IR spectra, which showed shifted S-H stretching frequencies (50–52). The acidity of MeSSH was also estimated in the context of the proton-

exchange method previously used to estimate the pK_a of cysteine persulfide (3, 53), yielding a ΔpK_a of 1.7 with CCSD/6-31 G (d′). Considering the pK_a of MeSH, 10.33 (19), a pK_a of 8.6 would be predicted for MeSSH.

Overall, our calculations follow the same trend as the experimental data and suggest that the factor that contributes the most to the lower pK_a of persulfides with respect to thiols is the weaker S-H bond in the persulfide compared with the thiol.

After determining the pK_a of GSSH, we analyzed the pH dependence of the apparent rate and equilibrium constants of Reaction 1 (Table S2 and Fig. S3). At pH 7.4, $k_{1,pH}$ is similar to $k_{1,ind}$ because most H_2S is ionized (p$K_{a\ H2S}$, 6.98) (38). In contrast, only a fraction of $k_{-1,ind}$ (~3600 M^{-1} s^{-1}) is evidenced at pH 7.4 (1.11 M^{-1} s^{-1}); $k_{-1,pH}$ decreases by deprotonation of GSSH (p$K_{a\ GSSH}$, 5.45) and protonation of GS^- (p$K_{a\ GSH}$, 8.94) (37). Thus, at pH 7.4, the apparent equilibrium constant $K_{eq1,pH\ 7.4}$ is 0.194, whereas $K_{eq1,ind}$ is 8.3×10^{-5}. This value of $K_{eq1,ind}$ corresponds to an endergonic $\Delta G°$ of +5.6 kcal/mol. The change in the apparent equilibrium constant at pH 7.4 translates into a difference of −4.6 kcal/mol. In other words, at pH 7.4, deprotonation of GSSH and protonation of GS^- drive Reaction 1 to the right.

The fact that $k_{-1,ind}$ is higher than $k_{1,ind}$, is consistent with GS^- being a better nucleophile than HS^- and GS^- being a poorer leaving group than HS^- (3), because H_2S has a lower pK_a than GSH. Furthermore, the unfavorable thermodynamics can be rationalized by better solvation of HS^- than GS^- and higher bond dissociation energy for the S-S bond in GSSG than GSSH (47, 49).

Kinetics of the reactions of GSSH with physiological electrophiles

The kinetics of the reactions of GSSH with peroxynitrite and H_2O_2 were studied using a pseudo-first-order excess of GSSH and the other components of the mixture. GSSH-containing mixtures were reacted with peroxynitrite (pH 7.23, 37 °C) and followed by the decrease in absorbance (Fig. 4*A*). The temperature was chosen to facilitate comparison with data reported for thiols (54). The k_{obs} obtained from peroxynitrite exponential decay correlated linearly with GSSH concentration (Fig. 4*B*). Precisely, the slope represents the sum of the contributions of the reactions of peroxynitrite with GSSH, GSH, and H_2S. The contributions of GSH and H_2S were calculated and subtracted from the global decay considering the rate constants at the working pH (1.29×10^3 M^{-1} s^{-1} for GSH (54), 7.93×10^3 M^{-1} s^{-1} for H_2S (38, 55, 56)) and the concentrations, which were measured separately. Thus, a $k_{pH\ 7.23}$ of $(1.25 \pm 0.03) \times 10^5$ M^{-1} s^{-1} was determined for the reaction of peroxynitrite and GSSH, 97 times higher than GSH under the same conditions. Given the pK_as of GSSH (5.45) and ONOOH (6.8) (56), k_{ind} was calculated to be $(4.7 \pm 0.1) \times 10^5$ M^{-1} s^{-1} with Equation 2. This value is 1.8 times higher than for GS^- (54, 56) (Table 1).

$$k_{pH} = k_{ind}\left(\frac{K_a^{RSSH}}{K_a^{RSSH} + [H^+]}\right)\left(\frac{[H^+]}{K_a^{ONOOH} + [H^+]}\right) \quad \text{(Eq. 2)}$$

The measurements of the kinetics of the reaction with H_2O_2 proved to be challenging, and the best results were obtained when peroxiredoxin 5 was used as a probe for H_2O_2. The fluorescence of peroxiredoxin 5 (Prx5) increases as it is oxidized by H_2O_2 (37, 57). Actually, a variant named Prx5v was used. This variant behaves similarly to WT with respect to the reaction with H_2O_2 but the formation of the disulfide from the sulfenic acid and the resolving cysteine is faster, minimizing parallel reactions of the sulfenic acid and improving the performance of the probe (Fig. S4). A GSSH-containing mixture was incubated with H_2O_2. Aliquots were taken at increasing times, diluted, and mixed with Prx5v. The intrinsic fluorescence of the enzyme, which is proportional to H_2O_2 (Fig. S5), was measured. From the k_{obs} of the decay of H_2O_2 in the presence of the mixture (Fig. 4*C*), after subtracting the contributions of GSH and H_2S to H_2O_2 decay (37, 38, 58), the $k_{pH\ 7.02}$ for the reaction of H_2O_2 and GSSH was determined to be 7.5 ± 0.6 M^{-1} s^{-1} (pH 7.02, 25 °C) (Fig. 4*C*). This value is 22 times higher than that of GSH under the same conditions. The k_{ind} of the reaction of GSS^- and H_2O_2 was calculated with Equation 3 considering that H_2O_2 does not ionize, because it has a pK_a of 11.62 (59). A value of 7.7 ± 0.6 M^{-1} s^{-1} was obtained, which is 4 times lower than the corresponding reaction of GS^- (37) (Table 1).

$$k_{pH} = k_{ind}\left(\frac{K_a^{RSSH}}{K_a^{RSSH} + [H^+]}\right) \quad \text{(Eq. 3)}$$

Computational insight into the reactions of persulfides and thiols with electrophiles

To provide a complementary microscopic insight into the reactivity of persulfide anions and thiolates, we studied computationally the reactions of the simplified models, MeS^- and $MeSS^-$, with mBrB, ONOOH, and H_2O_2. We employed a multi-scale QM/MM approach that allows to treat explicitly the solvent molecules while keeping the quantum nature needed for modeling the reactive species. This realistic representation of a chemical reaction in aqueous solution at room temperature enabled an accurate comparison between the simulations and the experimental data.

Inspection of the Gibbs energy profiles revealed that the transition states for both MeS^- and $MeSS^-$ were reached early. The geometries were almost identical (Fig. 5, *A–C*). The linear arrangement of the nucleophilic sulfur, the electrophilic center, and the closest atom of the leaving group suggests typical bimolecular nucleophilic substitutions (S_N2), as shown previously for thiolates (60, 61). A post-transition state proton transfer occurred in the case of H_2O_2 (37, 60, 62). The products were MeS-B/MeSS-B + Br^-, MeSOH/MeSSOH + NO_2^-, and $MeSO^-$/$MeSSO^-$ + H_2O, for the reactions with mBrB, ONOOH and H_2O_2, respectively. The reactions were strongly exergonic (Fig. 5, *D–F*).

The simulated activation Gibbs energies ($\Delta G^‡$, obtained from the maxima of the Gibbs energy profiles) for the reactions of MeS^-/$MeSS^-$ were compared with those calculated for GS^-/GSS^- from the experimental pH-independent rate constants k_{ind} according to the Transition State Theory (63) (Table

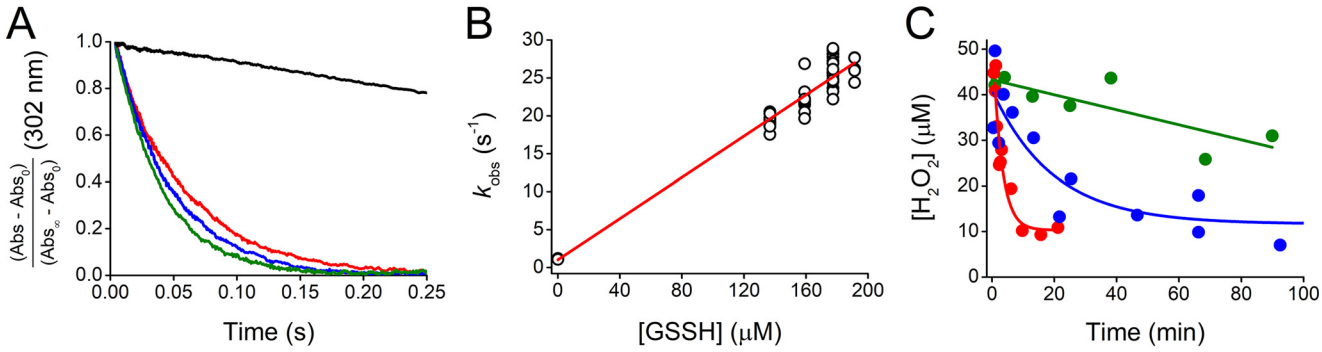

Figure 4. Kinetics of the reactions between GSSH and peroxynitrite or H_2O_2. *A*, reaction with peroxynitrite. Mixtures containing GSSH (137–191 μM), GSH (5.11 times GSSH), and H_2S (0.57 times GSSH) were mixed with 26 μM peroxynitrite (final concentrations) in phosphate buffer (0.1 M, pH 7.23, 37 °C, 0.1 mM dtpa) in a stopped-flow spectrophotometer. Normalized absorbance *versus* time. Representative time courses of peroxynitrite decay at 302 nm in the absence (*black*) or presence of 137 (*red*), 159 (*blue*), and 177 μM GSSH (*green*). Exponential plus linear functions were fitted to the time courses. Kinetic traces presented an increase in absorbance after seven half-lives, probably because of secondary reactions of H_2S (not shown) (55). *B*, k_{obs} *versus* GSSH concentration. The k_{obs} represents the sum of the contributions of the different decay processes, $k_{obs} = k_{pH\ GSSH}$ [GSSH] + $k_{pH\ GSH}$ [GSH] + $k_{pH\ H_2S}$ [H_2S] + $k_{pH\ peroxynitrite\ decay}$. The slope of (1.36 ± 0.03) × 10^5 M^{-1} s^{-1} (parameter ± error of the fit) is $k_{pH\ GSSH}$ + 5.11 $k_{pH\ GSH}$ + 0.57 $k_{pH\ H_2S}$. Then, the $k_{pH\ 7.23\ GSSH}$ was (1.25 ± 0.03) × 10^5 M^{-1} s^{-1}. The rate constant without GSSH-containing mixture was 1.13 ± 0.04 s^{-1} (mean ± S.D.), consistent with peroxynitrite spontaneous decay (99). The experiment shown is representative of four independent experiments. *C*, reaction with H_2O_2. Decay of 50 μM H_2O_2 in the presence of a mixture containing 0.71 mM GSSH, 2.0 mM GSH, and 0.37 mM H_2S (*red*), 2.0 mM GSH (*blue*), or 0.37 mM H_2S (*green*) in the same buffer (pH 7.02, 25 °C). Aliquots were diluted 100-fold and mixed with peroxiredoxin Prx5v (2–4 μM). The reactions were followed by the intrinsic fluorescence (λ_{ex} = 280 nm, λ_{em} = 340 nm) of Prx5v in phosphate buffer (50 mM, pH 7.4, 25 °C, 0.1 mM dtpa) in a plate reader. The exhibited time courses are representative experiments. The mean ± S.D. of three independent determinations yielded a k_{obs} of (6.2 ± 0.4) × 10^{-3} s^{-1} for H_2O_2 decay in the presence of the mixture, whereas the k_{obs} corresponding to GSH or H_2S controls were one or two orders of magnitude lower, respectively. Controls of Prx5v and GSH in the absence and presence of H_2O_2 showed no interference with the intrinsic fluorescence of the enzyme (not shown). The $k_{pH\ 7.02}$ for the reaction of H_2O_2 and GSSH was 7.5 ± 0.6 M^{-1} s^{-1} (see main text).

S3). The rate constant k relates to $\Delta G^{\ddagger}$ through Equation 4, where R is the ideal gas constant, T is the temperature, k_B and h are the Boltzmann and Plank constants, C° is 1 M, and τ is the transmission coefficient, assumed in this case to have a value of one.

$$k \approx \frac{\tau k_B T}{hC^{o}} e^{-\Delta G^{\ddagger}/RT} \qquad \text{(Eq. 4)}$$

The expected trends were observed for the Gibbs activation energies of the reactions with both thiolate and persulfide anion: $\Delta G^{\ddagger}_{H2O2} > \Delta G^{\ddagger}_{mBrB} > \Delta G^{\ddagger}_{ONOOH}$ (Table S3). When comparing MeS^- to $MeSS^-$, the differences in simulated $\Delta G^{\ddagger}$ were $\Delta\Delta G^{\ddagger}$ = 2.1 ± 0.9 for mBrB, 0.2 ± 0.8 for ONOOH, and 1.0 ± 0.8 kcal/mol for H_2O_2. These values are consistent with those determined from the experimental k_{ind} of 2.2, 0.5, and −0.8 kcal/mol, respectively (Table S3), although close to the reliability limit of the computational methodology. In fact, the $\Delta\Delta G^{\ddagger}$ of GS^-/GSS^- toward H_2O_2 was computationally estimated as 0.0 ± 0.5 kcal/mol (not shown). We evaluated the influence of the level of theory by performing calculations using an implicit solvent model with a variety of electronic structure schemes. The density functional theory (DFT) approach using the Perdew-Burke-Ernzerhof (PBE) functional employed in the QM/MM simulations, and more accurate electronic structure methods, showed similar differences when comparing the $\Delta G^{\ddagger}$ of MeS^- and $MeSS^-$ (Table S4).

We then evaluated the influence of the electronic structure of the species on the observed trends by monitoring Mulliken populations of selected atoms as a measure of charge distribution along the reactions. At the reactant complex, in the reactions with mBrB, the net −1 *e* charge was localized in MeS^- or $MeSS^-$, whereas with ONOOH and H_2O_2, the charge in MeS^- or $MeSS^-$ was approximately −0.85 to −0.90 *e* (Fig. 5, *G–I*). In every case, MeS^- exhibited the charge almost completely in its single sulfur atom whereas in $MeSS^-$ the charge was partitioned between both sulfur atoms. The largest redistributions of charges were observed around the transition states. The atoms constituting the leaving groups acquired a more negative charge, whereas the sulfur atoms became more positive. At the transition state, the atoms integrating MeS^- or $MeSS^-$ summed up a charge of approximately −0.59, −0.73, and −0.69 *e* (mean values for MeS^- and $MeSS^-$) in the reactions with mBrB, ONOOH, and H_2O_2, respectively (Table S5). The percent charge transferred from the reactant complex to the transition state had the same trend as $\Delta\Delta G^{\ddagger}$, mBrB > H_2O_2 > ONOOH (Table S3 and Table S5). Remarkably, the percent charge transferred was higher for $MeSS^-$ than MeS^- for the three electrophiles. In the case of mBrB, both the experimentally determined increase in nucleophilicity of GSS^- *versus* GS^- and the computed charge transferred in the transition state were the highest.

Finally, to monitor potential solvent effects, we computed radial correlation functions centered on the nucleophilic atoms. In the absence of an electrophile, the nucleophilic sulfur atoms of both MeS^- and $MeSS^-$ yielded the typical solvation patterns of diffuse anions (Fig. S6), consistent with previous work (60, 64). Their solvation structures became looser along the reaction as a consequence of the significant charge redistribution. The same effect was observed, to a lower extent, for the inner sulfur atom of $MeSS^-$ (not shown). No significant differences were found between MeS^- and $MeSS^-$ reactions with respect to the evolution of solvation patterns.

Overall, the relatively good correlation between the experimental and simulated data validates the use of $MeS^-/MeSS^-$ as simplified models. Our results suggest that the reactions occur through similar S_N2 mechanisms and that differences in reactivity are mainly due to electronic structure differences and not to solvent effects.

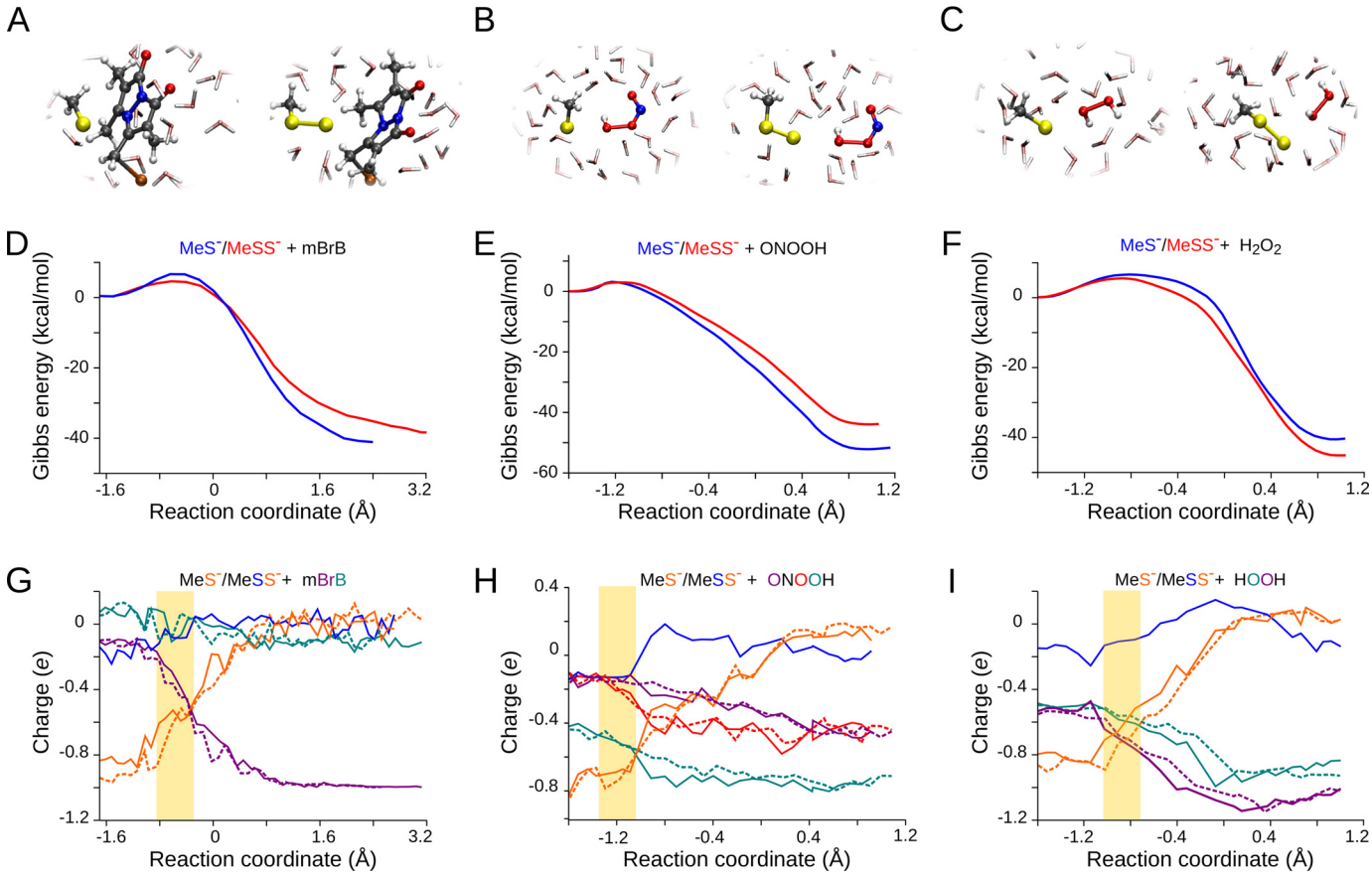

Figure 5. Transition states, Gibbs energy profiles, and evolution of charges. Reactions of MeS^- or $MeSS^-$ with mBrB (*panels A*, *D*, and *G*), ONOOH (*panels B*, *E*, and *H*), and H_2O_2 (*panels C*, *F*, and *I*) were studied by umbrella sampling in a QM/MM scheme. *A–C*, representative snapshots of the transition states of the thiolate (*left*) and persulfide anion (*right*). *D–F*, Gibbs energy profiles for MeS^- (*blue lines*) or $MeSS^-$ (*red lines*). *G–I*, average Mulliken populations as a function of reaction coordinate for MeS^- (*dashed lines*) or $MeSS^-$ (*solid lines*) reactions. Charges of atoms that exhibited significant variations are shown in the corresponding colors. The regions corresponding to the transition states are indicated with a *yellow box*.

α effect in persulfides

Brønsted plots correlate the nucleophilic capability with the basicity for a certain family of compounds according to Equation 5 (log of k_{ind} *versus* pK_a of the nucleophile), where β_{nuc}, typically between 0 and 1, is the Brønsted nucleophilic factor and C is a constant.

$$\log k_{ind} = \beta_{nuc}\, pK_a + C \qquad \text{(Eq. 5)}$$

Nucleophiles with high electron density in the atom adjacent to the nucleophilic atom show positive deviations from these plots and exhibit higher reactivity than expected according to their basicity (65). This deviation is known as the α effect.

Using our newly determined rate constants, the pK_a of GSSH, and published data for LMW thiols (37, 54, 56, 66), we constructed Brønsted plots (Fig. 6). Notably, the k_{ind} of GSS^- appeared above the trend reported for LMW thiolates with mBrB, ONOOH, and H_2O_2. The nucleophilicity of GSS^- was enhanced compared with that predicted for a thiolate with similar basicity by 1670-fold for mBrB, 50-fold for ONOOH, and 3.2-fold for H_2O_2 (Table 1).

The trend in the magnitude of the α effect (mBrB > ONOOH > H_2O_2) correlated with the β_{nuc} for the reactions of thiolates, which are 0.52 for mBrB, 0.42 for ONOOH, and 0.27 for H_2O_2 (37, 54, 66) (Table 1). These correlations have been previously observed for other nucleophile families (28, 67, 68) and are now observed for these sulfur nucleophiles. In addition, although comparisons between electrophiles of different types (*i.e.* centered in carbon or in oxygen) should be carried out with caution, a correlation was also observed between the α effect and the ability of the leaving group, which is related with the acidity of the conjugated acid (HBr > HNO_2 > H_2O, pK_as of −8.8, 3.35, and 14, respectively (69–71)). Note that in the reactions with H_2O_2 the proton transfer takes place after the transition state; thus, OH^- is the leaving group (37, 60, 62).

In summary, we evidenced the enhanced nucleophilicity of the biologically relevant persulfide GSS^- toward three electrophiles compared with the expected nucleophilicity of a thiolate of equal basicity. To our knowledge, our study represents the first examination of the α effect in sulfur nucleophiles.

Biological implications

The high acidity of GSSH (pK_a 5.45, 3.49 units below GSH), if extrapolated to other persulfide/thiol pairs, means that in biological systems the persulfides will be ionized whereas the thiols will be mainly protonated. The appearance of a negative charge could alter the functional properties of the original thiol. The situation may be different in particular proteins where the local environment may change the pK_a values.

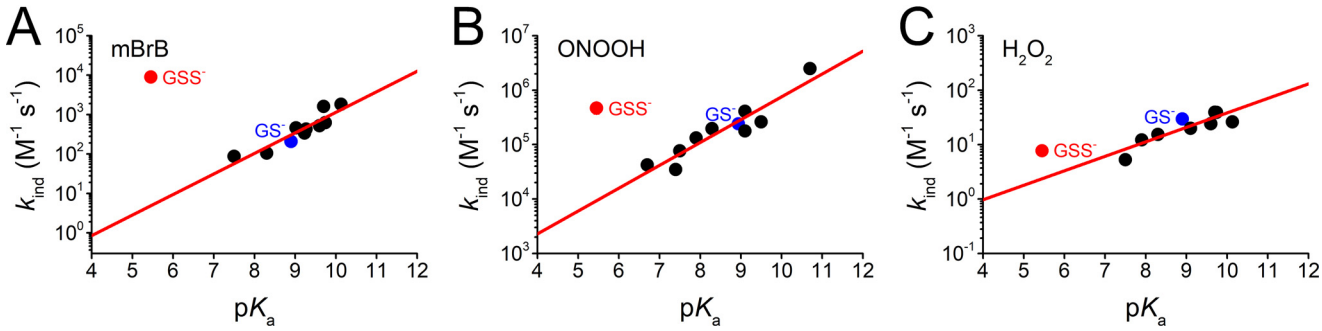

Figure 6. Comparison of the reactivity of GSS^- and thiolates with mBrB, ONOOH, and H_2O_2. Brønsted plots depicting the reported pH-independent rate constants (in logarithmic scale) *versus* thiol pK_a for the reactions of several LMW thiolates (*black circles*, GS^- in *blue*) with *A*, mBrB at 25 °C (β_{nuc} = 0.52 ± 0.08) (37); *B*, ONOOH at 37 °C (plot updated from (66) considering more recent pK_a estimations (37, 56); the fit yielded β_{nuc} = 0.42 ± 0.06 and C = 1.7 ± 0.5); and *C*, H_2O_2 at 25 °C (β_{nuc} = 0.27 ± 0.06) (37). The *red circles* show the pH-independent rate constants for GSS^- *versus* GSSH pK_a, reported herein.

The enhanced nucleophilic reactivity of GSSH compared with GSH at physiological pH is the result of two aspects, the higher availability of the ionized species due to its lower pK_a and, depending on the electrophile, the increased nucleophilicity of GSS^-. This is relevant for enzymatic (*i.e.* with persulfide dioxygenase) and nonenzymatic reactions (*i.e.* with one- and two-electron oxidants and other electrophiles) in which GSSH acts as a nucleophile. Extrapolation to other persulfide/thiol pairs would indicate an enhancement in reactivity of one to three orders of magnitude (Table 1), which could vary depending on the specific molecular environment, the pH, and the electrophilic partner. The relatively high nucleophilic reactivity of persulfides could contribute to the proposed protective effects of persulfidation. Oxidation of persulfides can lead to products (*i.e.* $RSSO_2H$ and $RSSO_3H$) that can be reduced by cellular reductants systems, whereas analogous oxidation of thiols yields irreversible oxidation products (*i.e.* RSO_2H and RSO_3H) (4, 16, 24, 44).

Importantly, the biological properties of persulfides can also be attributed to their electrophilicity, as in transpersulfidation reactions, which is a property absent in thiols. It is likely that both the enhanced nucleophilicity and the electrophilicity contribute to the persulfide-mediated downstream effects of H_2S.

Our analysis of persulfide pK_a and nucleophilicity has implications for the reaction catalyzed by the mitochondrial enzyme SQOR. It has been proposed that this enzyme contains a trisulfide (RSSSR) instead of a disulfide (RSSR) in its two active site cysteines (72). Reaction of H_2S with RSSSR instead of RSSR to form two persulfides could imply an acceleration of ~two orders of magnitude, because persulfide is a better leaving group than thiol because of its lower pK_a (3). In the following step of the reaction, which involves the attack of the enzyme-formed persulfide or thiolate on the electrophilic FAD cofactor, an acceleration of one to three orders of magnitude would be expected for the persulfide. These estimations are based on considerations for LMW species; as is typical with enzymes, specific protein effects could lead to further acceleration factors. In fact, recent computational estimations suggest a rate increase of ~10^5-fold for the first step if the active site of SQOR is in the trisulfide instead of the disulfide state (73).

Conclusions

This study reveals several aspects about the formation, acidity, and nucleophilicity of GSSH, summarized as follows. 1) A reversed-phase HPLC method based on mBrB derivatization can be used for quantification of GSSH in mixtures. 2) Excess GSSG and H_2S generate GSSH, GSH, and GSSSG through at least two reversible reactions, Reaction 1 (GSSG + H_2S) and Reaction 2 (GSSG + GSSH). At physiological pH and 25 ± 1 °C, the rate constants are $k_{1,pH}$ = 0.23 ± 0.02, $k_{-1,pH}$ = 1.11 ± 0.06, $k_{2,pH}$ = 1.6-2.3, and $k_{-2,pH}$ = 3.1-9 M^{-1} s^{-1}. 3) The apparent equilibrium constant $K_{eq1,pH}$ is 0.194 ± 0.005 (pH 7.4, 25 ± 1 °C). 4) The reaction of GSSG with HS^- to form GSSH and GS^- is endergonic but is driven by −4.6 kcal/mol through deprotonation of GSSH and protonation of GS^- at physiological pH. 5) In mixtures of GSSG and H_2S, the formation of GSSH is not stoichiometric with respect to GSH nor to the initial concentration of H_2S because the products undergo subsequent reactions. 6) The pK_a of GSSH is 5.45 ± 0.03, 3.49 units below the pK_a of GSH. This is, to our knowledge, the first report of the pK_a of a biological persulfide. 7) The higher acidity of persulfides compared with thiols is due mainly to the weaker S-H bond. 8) At physiological pH, GSSH reacts 1200, 97, and 22 times more rapidly than GSH with the electrophiles mBrB, peroxynitrite, and H_2O_2, respectively. This can be explained by the increased availability of the ionized species and, depending on the electrophile, by the increased nucleophilicity. 9) The reactions of GSSH occur through S_N2 mechanisms similar to those of thiols. 10) The differences in reactivity are related to the electronic structures of the species rather than to solvent effects. 11) The α effect is evidenced by the positive deviation in Brønsted plots. 12) The increased reactivity of GSS^- compared with a thiolate of similar basicity is 1670-fold with mBrB, 50-fold with ONOOH, and 3.2-fold with H_2O_2. 13) The magnitude of the α effect varies with the electrophile. It correlates with the β_{nuc} for the reactions with thiolates and with the ability of the leaving groups. An examination of the α effect in sulfur nucleophiles is unprecedented to our knowledge. Overall, our study contributes to the understanding of the basic chemical properties of persulfides, which affects their roles in biosynthesis, catabolism, and H_2S signaling.

Experimental procedures

Reagents and solutions

Solutions of GSSG (AppliChem) were prepared in sodium phosphate buffer (0.1 M, pH 7.4). When specified, the buffer also contained 0.1 mM diethylenetriamine pentaacetic acid (dtpa, ACROS). Depending on the desired final pH, 1.5–2 equivalents of NaOH were added. GSH (ACROS) was dissolved in the mentioned buffer. Crystals of $Na_2S{\cdot}9H_2O$ (Carlo Erba), stored under argon in a desiccator, were washed with distilled water, dissolved in ultrapure water, and used within a few hours. Solutions containing H_2S were prepared in sealed vials with minimum headspace and manipulated with gas-tight Hamilton syringes. Concentrated stocks of mBrB (Sigma-Aldrich) (50 mM) were prepared in acetonitrile; dilutions (<120 μM) were freshly prepared in ultrapure water or buffer and quantified by absorbance at 396 nm (ϵ_{396} = 5300 M^{-1} cm^{-1}) (74). Solutions of TCEP (Sigma-Aldrich) were prepared in distilled water. Solutions of H_2O_2 (BAKER) were prepared in ultrapure water and quantified by absorbance at 240 nm (ϵ_{240} = 39.4 M^{-1} cm^{-1}) (75, 76). Peroxynitrite stocks were prepared as previously and quantified by absorbance at 302 nm (ϵ_{302} = 1700 M^{-1} cm^{-1}) (56, 77, 78); dilutions (26 μM) were freshly prepared in 2 mM NaOH.

Reversed-phase HPLC

Reversed-phase chromatography was performed using a 1260 Infinity HPLC (Agilent) with a diode array UV-visible absorbance detector and a C18 Ascentis column (100 × 4.6 mm, 3 μm, Sigma-Aldrich). Samples derivatized with mBrB were diluted 2-fold in 0.1% (v/v) TFA (Fluka) prior to injection and eluted with a gradient of 0.1% (v/v) TFA:acetonitrile (100:0 from 0 to 2 min, 60:40 from 8 to 10 min, 5:95 from 12 to 14 min) at a flow rate of 0.8 ml/min. Chromatograms were recorded at 260 and 396 nm.

MS

Fractions collected from the HPLC underwent two cycles of evaporation in a vacuum concentrator to remove the TFA and redissolved in ultrapure water. The aqueous fractions were then diluted in 0.1% (v/v) formic acid and analyzed by direct infusion into a hybrid triple-quadrupole/linear ion trap mass spectrometer (QTRAP4500, AB Sciex). Mass spectrometer parameters were optimized for best signal quality according to the corresponding analyte and method. For molecular ion identification, Q1 mode was employed in positive mode, electrospray voltage and declustering potential were set to 5.5 kV and 70 V, respectively, and the scan speed was set to 1000 Da/s. Fragmentation experiments were performed in the Product Ion mode with a collision energy ramp from 20 to 50 V. Data were acquired with Analyst 1.6.2 software and analyzed with PeakView 2.2 (AB Sciex).

Kinetics and equilibrium studies followed by HPLC

To study the reaction between GSSG and H_2S, 5–11 mM GSSG and 0.5 mM H_2S were incubated for increasing time periods in sodium phosphate buffer (0.1 M, pH 7.4, 25 ± 1 °C). In another set of experiments, 5 mM GSSG and 0.5 mM H_2S were preincubated for 1 h in the mentioned buffer; then, 2–12.5 mM GSH was added, leaving minimum headspace in the vial. At the end of the experiments, the final pHs of the reaction mixtures were measured. In both sets of experiments, aliquots were taken at different incubation times and the reactions were stopped by 2.5- to 9.5-fold dilution in 4 or 10 mM mBrB, final concentrations, in sodium phosphate buffer (80–95 mM, pH 7.4). The derivatized samples were then analyzed by HPLC. For GSSG, the chromatograms at 260 nm were used, whereas for the other species, the chromatograms at 396 nm corresponding to the bimane derivatives were used. The concentrations of GSSG, GSH, GSSH, and H_2S were determined by measurement of the area under the peaks and comparison with calibration curves of known standards. Considering that the bimane derivatives of GSSH and GSH have the same absorptivity because of the bimane moieties, the calibration curve for GSH was used to quantify GSSH. OriginPro 8.6 was used to analyze data. COPASI (40), a software application for the simulation and analysis of biochemical networks, was used to simulate time courses and fit kinetic parameters. Parameters in COPASI were estimated with the Levenberg-Marquardt algorithm.

To characterize the apparent equilibrium constant, $K_{eq1,pH}$, 6–10 mM GSSG and 0.5 mM H_2S were incubated in sodium phosphate buffer (0.1 M, pH 7.4, 25 °C), under shaking, in glass insert tubes inside sealed vials with almost no headspace. After 2 h, 4 mM mBrB was added and the samples were analyzed by HPLC.

Determination of the pK_a of GSSH

The pK_a of GSSH was determined by the pH dependence of the reaction with mBrB using both an initial rate approach, as previously described for thiols, and an integral method under pseudo-first-order conditions with mBrB in excess (48). A three-component, constant ionic strength (I = 0.15 M) buffer was used in the pH range of 4.16–7.41 (79). The buffer (1×) contained 15 mM acetic acid (Dorwil, Argentina), 15 mM MES (Applichem), 30 mM Tris (Applichem), 120 mM NaCl (Applichem), 0.1 mM dtpa, and variable amounts of HCl or NaOH to adjust the pH.

In the initial rate approach, stock solutions of mBrB and mixtures of 10 mM GSSG and 2 mM H_2S, which had been incubated for 1 h in sodium phosphate buffer (0.1 M, pH 7.4) to form GSSH, were freshly diluted in ultrapure water immediately before use. The initial rates of the reaction between 1 μM mBrB and mixtures that contained ~0.75 μM GSSH (final concentrations) were measured in a Varioskan Flash plate reader (Thermo Fisher Scientific) at 25 °C. In a 384-well black plate, 11 or 12 reactions at different pHs were prepared in quadruplicate. Each well contained 20 μl of the three-component buffer 5× and 50 μl of the diluted GSSH-containing mixture. The reactions were started by the injection of 30 μl of mBrB using the automatic dispenser of the plate reader. Fluorescence (λ_{ex} = 396 nm, λ_{em} = 472 nm) was measured during 5–13 min and linear functions were fitted to the readings. The obtained slope, which is proportional to the initial rate, was determined for each pH. To evaluate buffer interference, controls without the

GSSH-containing mixture were performed. The pHs of the solutions were measured immediately after the reactions. An aliquot of the GSSH-containing mixture was derivatized with 9 mM mBrB for HPLC analysis.

In pseudo-first-order experiments, rapid kinetics were studied in the presence of excess mBrB in a stopped-flow spectrofluorimeter (Applied Photophysics SX20). To prepare GSSH-containing mixtures, 10 mM GSSG and 2 mM H_2S were preincubated for at least 1 h in sodium phosphate buffer (0.1 M, pH 7.4, 0.1 mM dtpa) and then diluted in ultrapure water immediately before use. The diluted GSSH-containing mixtures (~2 μM GSSH) were reacted with 18–81 μM mBrB, final concentrations, prepared in the three-component buffer 2× at different pHs at 25 °C. The fluorescence (λ_{ex} = 396 nm, emission cutoff 435 nm) of the product was recorded during 18–500 s. The final pHs were measured. At pH 7.40, experiments were also performed in sodium phosphate buffer (0.1 M, 0.1 mM dtpa) and included controls with 118 μM mBrB and 6.3 μM GSH or buffer alone. The data were analyzed with OriginPro 8.6 or Pro-Data SX20 software (Applied Photophysics).

Kinetics of the reaction of GSSH with peroxynitrite

The kinetics of the reaction was studied under pseudo-first-order conditions with excess GSSH. The decay of peroxynitrite was followed by the decrease in absorbance at 302 nm in the stopped-flow. To prepare GSSH, 10 mM GSSG and 2 mM H_2S were preincubated for 1.5 h in sodium phosphate buffer (0.2 M, pH 7.4, 0.2 mM dtpa) at 25 °C. The GSSH-containing mixtures were diluted up to 1.4-fold in the mentioned buffer (137–191 μM) minimizing headspace and were reacted with freshly prepared solutions of 26 μM peroxynitrite, final concentrations, at 37 °C. The pH was measured at the end of each reaction. The peroxynitrite-dependent change in absorbance at 302 nm was recorded for 1 s. Controls of the spontaneous decay of peroxynitrite in buffer alone were performed under the same conditions. In parallel, aliquots of the GSSH-containing mixtures were separated for HPLC quantification of GSSH, GSH, and H_2S. Data were analyzed with the software OriginPro 8.6.

Kinetics of the reaction of GSSH with H_2O_2

The decay of H_2O_2 was monitored using Prx5 as a sensor of H_2O_2 because the intrinsic fluorescence of this enzyme increases with oxidation (37, 57). The Prx5 variant (Prx5v) that was used contained an N-terminal 6×His-Tag and extra residues in the C-terminal end. The molecular mass of this protein was verified by SDS-PAGE and MALDI-TOF MS. The sequence was verified by trypsin digestion and MALDI-TOF MS and MS/MS analysis of the tryptic peptides (4800 MALDI-TOF/TOF, AB Sciex). The fast reaction with H_2O_2 was characterized (Fig. S4). Prx5v reacted with H_2O_2 with a similar rate constant to WT ($(2.9 \pm 0.7) \times 10^5$ M^{-1} s^{-1}, pH 7.1, 25 °C). Nevertheless, the formation of the disulfide from the sulfenic acid and the resolving cysteine was faster than in WT (127 ± 2 s^{-1}, pH 7.1, 25 °C, for Prx5v *versus* 14.7 s^{-1}, pH 7.4, 25 °C (57) or 21 s^{-1}, pH 6.9, 25 °C (37), for WT). This minimizes parallel reactions of the sulfenic acid and improves probe performance.

To prepare GSSH-containing mixtures, 10 mM GSSG was preincubated with 2 mM H_2S in sodium phosphate buffer (0.1 M, pH 7.4, 0.1 mM dtpa). After 1.5 h, 50 μM H_2O_2 was added. Aliquots of 2 μl were taken at increasing incubation times and mixed with 198 μl of reduced Prx5v (2–4 μM) in sodium phosphate buffer (50 mM, pH 7.4, 0.1 mM dtpa). Fluorescence (λ_{ex} = 280, λ_{em} = 340 nm) was immediately measured in a Varioskan Flash plate reader at 25 °C. Then, the pH of the reaction mixtures was measured. Calibration curves of H_2O_2 were simultaneously done in each experiment using the same dilution of reduced Prx5v (Fig. S5). Prior to the reaction with H_2O_2, an aliquot of the GSSH-containing mixture was analyzed by HPLC for quantification of GSSH, GSH, and H_2S. Controls with the concentrations of GSH or H_2S equivalent to those present in the GSSH-containing mixtures were performed under the same conditions. Data were analyzed using the software OriginPro 8.6.

The decay of H_2O_2 in the presence of excess GSSH was studied by two additional methods that yielded rate constants within the same order of magnitude as Prx5v (not shown), namely the formation of oxygen in the presence of catalase in an oxymeter and the fluorescence produced by Amplex UltraRed oxidation by H_2O_2 in the presence of horseradish peroxidase. Methods based on Amplex Red and xylenol orange essays had interference from species present in the mixtures.

Computational methods

$MeSH/MeS^-$ and $MeSSH/MeSS^-$ were used as models of thiol and persulfide, respectively. Electronic structure calculations were performed with Gaussian09 (80) whereas QM/MM molecular dynamics (MD) simulations were performed using LIO (https://github.com/MALBECC/LIO), a software developed by the Group of Molecular Modeling in the Universidad de Buenos Aires, compiled with Amber14 (81, 82). Dynamics visualizations and molecular drawings were performed with VMD 1.9.1 (83).

Computational comparison of the acidity of persulfides and thiols

All structures were optimized using DFT-based methodology. Computations were performed at the generalized gradient approximation level, using the PBE combination of exchange and correlation functional with a double-zeta plus polarization (dzvp) Gaussian basis set (84, 85). Frequency calculations were performed in each case and Gibbs energy changes were estimated by means of standard statistical mechanics formalism. The polarizable continuum solvent model was employed with the default parameters of aqueous solvation (86). Additionally, electronic structure calculations were performed employing the Møller-Plesset perturbation theory (at the MP2 level) with dzvp basis, and the ωB97x-D and M062X methods combined with a 6-31 G(d') basis set, which have been reported to yield good accuracy for thermochemistry and kinetic applications where noncovalent interactions are significant (87–89). Finally, we repeated the simulations with a more accurate CCSD methodology, also employing a 6-31 G(d') basis set.

Initial survey of the system in vacuum and implicit solvent

Structures of reactant complexes, transition states, and product complexes were optimized *in vacuo* and using polarizable continuum solvent model with aqueous solvation default parameters (86) at the DFT level. Computations were performed at the generalized gradient approximation level, using the PBE combination of exchange and correlation functional, with a dzvp Gaussian basis set (84, 85). Frequency calculations were performed in each case to ensure that the obtained structures for reactant complexes and product complexes corresponded to minima in the potential energy surface. Transition-state structures were confirmed by exploring the intrinsic reaction coordinate (90). Gibbs energies were estimated by means of standard statistical mechanics formalism, as implemented in the Gaussian09 suite. Single-point calculations on the PBE/dzvp optimized structures were calculated employing Møller-Plesset perturbation theory (at the MP2 level) with dzvp basis to evaluate activation barrier underestimations inherent to pure DFT functionals. We also employed the ωB97X-D and M062X methods combined with a 6-31 G(d') basis set, which have been reported to yield good accuracy for thermochemistry and kinetics applications where noncovalent interactions are significant (88, 89).

Multi-scale QM/MM MD: preparation of the initial system

Reactants were described by QM at the DFT PBE/dzvp level of theory and solvated with explicit classical (MM) water molecules described with the TIP3P model (91) in a truncated 25-Å octahedral box. Initial structures for the reactants were those previously optimized in Gaussian09 at the same level of theory. Periodic boundary conditions were used. The Lennard-Jones parameters (ϵ and σ) for the QM subsystem atoms were those of the general AMBER force field, *i.e.* 0.3200, 0.2500, 0.2104, 0.1700, 0.1094, and 0.0157 kcal/mol, and 2.220, 2.000, 1.7210, 1.8240, 1.9080, and 1.4870 Å, for Br, S, O, N, C, and H atoms, respectively (92). The system was relaxed optimizing first only the atoms integrating the QM subsystem, maintaining the MM subsystem fixed, and then optimizing both the QM and MM subsystems. Next, the MM subsystem was heated from 0 to 300 K during 0.1 ns of MM MD with the Berendsen thermostat (93), followed by a 1-ps-long QM/MM MD employing an uncoupled Berendsen thermostat, to ensure a reliable thermalization of the full system and to control the local kinetic energy of the relatively small QM subsystem.

Multi-scale QM/MM MD: Calculation of Gibbs energy profiles

Gibbs energy profiles were obtained with the umbrella sampling method (94, 95). The reaction coordinate was defined as the difference in the distance between the nucleophilic sulfur atom and the electrophilic center (the carbon atom bound to bromine in mBrB and the H-bonded oxygen in ONOOH and H_2O_2) and the distance between the electrophilic center and the closest atom of the leaving group.

Initial structures for the umbrella sampling calculations were extracted from a 25-ps-long steered QM/MM MD using a force constant of 200 kcal/mol/Å^2. Windows were centered at different reaction coordinate reference values, spaced by 0.1 Å in most cases. Then, a quadratic bias potential function also centered in the reference values was added to the reaction coordinate, and the windows were carefully relaxed following a protocol that combined classical MD and QM/MM optimizations to improve solvation sampling at an affordable computational cost (96). A 5-ps-long QM/MM MD simulation was generated of each window with the uncoupled Berendsen thermostat, and then another 5-ps QM/MM MD simulation was performed employing the stochastic Langevin thermostat to ensure a canonical distribution (97). Finally, Gibbs energy profiles were computed employing the Langevin MD data and the umbrella integration method (98).

Data availability

The data that support the findings of this study are contained within this article and in the supporting information. Raw data are available upon request (mmoller@fcien.edu.uy, dario@qi.fcen.uba.ar, beatriz.alvarez@fcien.edu.uy).

Acknowledgments—We thank Adriana Cassina and Stephanie Portillo-Ledesma (Universidad de la República) for help with oximetry and Prx5v experiments, respectively.

Author contributions—D. B., J. A. S., E. C., G. F.-S., M. N. M., and B. A. investigation; D. B., J. A. S., and B. A. writing-original draft; D. B., J. A. S., E. C., G. F.-S., A. Z., M. T., M. N. M., D. A. E., and B. A. writing-review and editing; E. C., G. F.-S., A. Z., M. T., M. N. M., D. A. E., and B. A. conceptualization; E. C., A. Z., M. T., D. A. E., and B. A. supervision; M. M., J. S. G., G. F.-S., M. N. M., and D. A. E. methodology; D. A. E. and B. A. funding acquisition; D. A. E. and B. A. project administration.

Funding and additional information—This work was supported in part by Comisión Sectorial de Investigación Científica (CSIC), Universidad de la República, Grants GRUPOS_2014_C632-348, GRUPOS_2018_47, I+D_2016_541 (to B. A.) and I+D 2016_367 (to M. T.), Espacio Interdisciplinario, Universidad de la República, Grant Centros_2015, Agencia Nacional de Investigación e Innovación (ANII), Uruguay, Grant FCE_1_2017_1_136043 (to M. N. M), Fondo Vaz Ferreira, Ministerio de Educación y Cultura, Uruguay, Grants I/FVF2017/069 (to E. C.) and I/FVF2017/185 (to A. Z.), Universidad de Buenos Aires Grant UBACYT 20020130100097BA, Agencia Nacional de Promoción Científica y Tecnológica, Argentina, Grants PICT 2014-1022 and PICT 2015-2761, and Consejo Nacional de Investigaciones Científicas y Técnicas (CONICET), Argentina, Grant 11220150100303CO. D. B., E. C., and M. M. were partially supported by Comisión Académica de Posgrado, Universidad de la República, and by PEDECIBA, Uruguay. J. A. S. was partially supported by Consejo Nacional de Investigaciones Científicas y Técnicas (CONICET), Argentina, and Programa Escala Docente, Asociación de Universidades Grupo Montevideo. The computer simulations were performed at CECAR and Instituto de Química Física de los Materiales, Medio Ambiente y Energía (INQUIMAE) clusters, Facultad de Ciencias Exactas y Naturales, Universidad de Buenos Aires.

Conflict of interest—The authors declare that they have no conflicts of interest with the contents of this article.

Abbreviations—The abbreviations used are: RSSH, hydropersulfide; GSH, glutathione; GSSH, glutathione persulfide; GSSG, glutathione disulfide; GSSSG, glutathione trisulfide; mBrB, monobromobimane; GS-B, GSH derivatized with mBrB; GSS-B, GSSH derivatized with mBrB; B-S-B, H_2S derivatized with mBrB; MeSH, methanethiol; MeSSH, methane hydropersulfide; MeS^-, methanethiolate; $MeSS^-$, methanepersulfide anion; ONOOH, peroxynitrous acid; LMW, low molecular weight; SQOR, sulfide quinone oxidoreductase; Prx5, peroxiredoxin 5; Prx5v, peroxiredoxin 5 variant; QM, quantum mechanics; MM, molecular mechanics; MD, molecular dynamics; CCSD, coupled cluster singles and doubles method; DFT, density functional theory; dzvp, double-zeta plus polarization; PCM, polarizable continuum model; TCEP, tris(2-carboxyethyl) phosphine; dtpa, diethylenetriamine pentaacetic acid; PBE, Perdew-Burke-Ernzerhof.

References

1. Filipovic, M. R., Zivanovic, J., Alvarez, B., and Banerjee, R. (2018) Chemical biology of H_2S signaling through persulfidation. *Chem. Rev.* **118,** 1253–1337 CrossRef Medline
2. Mueller, E. G. (2006) Trafficking in persulfides: delivering sulfur in biosynthetic pathways. *Nat. Chem. Biol.* **2,** 185–194 CrossRef Medline
3. Cuevasanta, E., Lange, M., Bonanata, J., Coitiño, E. L., Ferrer-Sueta, G., Filipovic, M. R., and Alvarez, B. (2015) Reaction of hydrogen sulfide with disulfide and sulfenic acid to form the strongly nucleophilic persulfide. *J. Biol. Chem.* **290,** 26866–26880 CrossRef Medline
4. Greiner, R., Pálinkás, Z., Bäsell, K., Becher, D., Antelmann, H., Nagy, P., and Dick, T. P. (2013) Polysulfides link H_2S to protein thiol oxidation. *Antioxid. Redox Signal.* **19,** 1749–1765 CrossRef Medline
5. Zhang, D., Macinkovic, I., Devarie-Baez, N. O., Pan, J., Park, C.-M., Carroll, K. S., Filipovic, M. R., and Xian, M. (2014) Detection of protein S-sulfhydration by a tag-switch technique. *Angew. Chem. Int. Ed Engl.* **53,** 575–581 CrossRef Medline
6. Yadav, P. K., Yamada, K., Chiku, T., Koutmos, M., and Banerjee, R. (2013) Structure and kinetic analysis of H_2S production by human mercaptopyruvate sulfurtransferase. *J. Biol. Chem.* **288,** 20002–20013 CrossRef Medline
7. Ida, T., Sawa, T., Ihara, H., Tsuchiya, Y., Watanabe, Y., Kumagai, Y., Suematsu, M., Motohashi, H., Fujii, S., Matsunaga, T., Yamamoto, M., Ono, K., Devarie-Baez, N. O., Xian, M., Fukuto, J. M., *et al.* (2014) Reactive cysteine persulfides and S-polythiolation regulate oxidative stress and redox signaling. *Proc. Natl. Acad. Sci. U. S. A.* **111,** 7606–7611 CrossRef Medline
8. Yadav, P. K., Martinov, M., Vitvitsky, V., Seravalli, J., Wedmann, R., Filipovic, M. R., and Banerjee, R. (2016) Biosynthesis and reactivity of cysteine persulfides in signaling. *J. Am. Chem. Soc.* **138,** 289–299 CrossRef Medline
9. Akaike, T., Ida, T., Wei, F.-Y., Nishida, M., Kumagai, Y., Alam, M. M., Ihara, H., Sawa, T., Matsunaga, T., Kasamatsu, S., Nishimura, A., Morita, M., Tomizawa, K., Nishimura, A., Watanabe, S., *et al.* (2017) Cysteinyl-tRNA synthetase governs cysteine polysulfidation and mitochondrial bioenergetics. *Nat. Commun.* **8,** 1177 CrossRef Medline
10. Hildebrandt, T. M., and Grieshaber, M. K. (2008) Three enzymatic activities catalyze the oxidation of sulfide to thiosulfate in mammalian and invertebrate mitochondria. *FEBS J.* **275,** 3352–3361 CrossRef Medline
11. Jackson, M. R., Melideo, S. L., and Jorns, M. S. (2012) Human sulfide:quinone oxidoreductase catalyzes the first step in hydrogen sulfide metabolism and produces a sulfane sulfur metabolite. *Biochemistry* **51,** 6804–6815 CrossRef Medline
12. Libiad, M., Yadav, P. K., Vitvitsky, V., Martinov, M., and Banerjee, R. (2014) Organization of the human mitochondrial hydrogen sulfide oxidation pathway. *J. Biol. Chem.* **289,** 30901–30910 CrossRef Medline
13. Kabil, O., and Banerjee, R. (2012) Characterization of patient mutations in human persulfide dioxygenase (ETHE1) involved in H2S catabolism. *J. Biol. Chem.* **287,** 44561–44567 CrossRef Medline
14. Tiranti, V., Viscomi, C., Hildebrandt, T., Di Meo, I., Mineri, R., Tiveron, C., Levitt, M. D., Prelle, A., Fagiolari, G., Rimoldi, M., and Zeviani, M. (2009) Loss of ETHE1, a mitochondrial dioxygenase, causes fatal sulfide toxicity in ethylmalonic encephalopathy. *Nat. Med.* **15,** 200–205 CrossRef Medline
15. Melideo, S. L., Jackson, M. R., and Jorns, M. S. (2014) Biosynthesis of a central intermediate in hydrogen sulfide metabolism by a novel human sulfurtransferase and its yeast ortholog. *Biochemistry* **53,** 4739–4753 CrossRef Medline
16. Dóka, É., Ida, T., Dagnell, M., Abiko, Y., Luong, N. C., Balog, N., Takata, T., Espinosa, B., Nishimura, A., Cheng, Q., Funato, Y., Miki, H., Fukuto, J. M., Prigge, J. R., Schmidt, E. E., *et al.* (2020) Control of protein function through oxidation and reduction of persulfidated states. *Sci. Adv.* **6,** eaax8358 CrossRef Medline
17. Everett, S. A., Folkes, L. K., Wardman, P., and Asmus, K. D. (1994) Free-radical repair by a novel perthiol: reversible hydrogen transfer and perthiyl radical formation. *Free Radic. Res.* **20,** 387–400 CrossRef
18. Chauvin, J.-P. R., Griesser, M., and Pratt, D. A. (2017) Hydropersulfides: H-atom transfer agents par excellence. *J. Am. Chem. Soc.* **139,** 6484–6493 CrossRef Medline
19. Serjeant, E. P., and Dempsey, B. (1979) *Ionisation constants of organic acids in aqueous solution*. Pergamon Press, New York
20. Benaïchouche, M., Bosser, G., Paris, J., and Plichon, V. (1990) Relative nucleophilicities of aryldisulphide and thiolate ions in dimethylacetamide estimated from their reaction rates with alkyl halides. *J. Chem. Soc. Perkin Trans. 2* 1421–1424 CrossRef
21. Cuevasanta, E., Reyes, A. M., Zeida, A., Mastrogiovanni, M., De Armas, M. I., Radi, R., Alvarez, B., and Trujillo, M. (2019) Kinetics of formation and reactivity of the persulfide in the one-cysteine peroxiredoxin from *Mycobacterium tuberculosis*. *J. Biol. Chem.* **294,** 13593–13605 CrossRef Medline
22. Everett, S. A., and Wardman, P. (1995) Perthiols as antioxidants: radical-scavenging and prooxidative mechanisms. *Methods Enzymol.* **251,** 55–69 CrossRef Medline
23. Francoleon, N. E., Carrington, S. J., and Fukuto, J. M. (2011) The reaction of H(2)S with oxidized thiols: generation of persulfides and implications to H(2)S biology. *Arch. Biochem. Biophys.* **516,** 146–153 CrossRef Medline
24. Ono, K., Akaike, T., Sawa, T., Kumagai, Y., Wink, D. A., Tantillo, D. J., Hobbs, A. J., Nagy, P., Xian, M., Lin, J., and Fukuto, J. M. (2014) Redox chemistry and chemical biology of H_2S, hydropersulfides, and derived species: implications of their possible biological activity and utility. *Free Radic. Biol. Med.* **77,** 82–94 CrossRef Medline
25. Gold, V. (1983) Glossary of terms used in physical organic chemistry. *Pure Appl. Chem.* **55,** 1281–1371 CrossRef
26. Garver, J. M., Gronert, S., and Bierbaum, V. M. (2011) Experimental validation of the α-effect in the gas phase. *J. Am. Chem. Soc.* **133,** 13894–13897 CrossRef Medline
27. Edwards, J. O., and Pearson, R. G. (1962) The factors determining nucleophilic reactivities. *J. Am. Chem. Soc.* **84,** 16–24 CrossRef
28. Hoz, S. (1982) The α effect: on the origin of transition-state stabilization. *J. Org. Chem.* **47,** 3545–3547 CrossRef
29. Um, I.-H., Im, L.-R., and Buncel, E. (2010) Pitfalls in assessing the α-effect: Reactions of substituted phenyl methanesulfonates with HOO−, OH−, and substituted phenoxides in H_2O. *J. Org. Chem.* **75,** 8571–8577 CrossRef Medline
30. Bogdándi, V., Ida, T., Sutton, T. R., Bianco, C., Ditrói, T., Koster, G., Henthorn, H. A., Minnion, M., Toscano, J. P., van der Vliet, A., Pluth, M. D., Feelisch, M., Fukuto, J. M., Akaike, T., and Nagy, P. (2019) Speciation of reactive sulfur species and their reactions with alkylating agents: do we have any clue about what is present inside the cell? *Br. J. Pharmacol.* **176,** 646–670 CrossRef Medline
31. Pan, J., and Carroll, K. S. (2013) Persulfide reactivity in the detection of protein S-sulfhydration. *ACS Chem. Biol.* **8,** 1110–1116 CrossRef Medline

32. Vasas, A., Dóka, É., Fábián, I., and Nagy, P. (2015) Kinetic and thermodynamic studies on the disulfide-bond reducing potential of hydrogen sulfide. *Nitric Oxide Biol. Chem.* **46,** 93–101 CrossRef Medline
33. Kosower, N. S., Kosower, E. M., Newton, G. L., and Ranney, H. M. (1979) Bimane fluorescent labels: labeling of normal human red cells under physiological conditions. *Proc. Natl. Acad. Sci. U. S. A.* **76,** 3382–3386 CrossRef Medline
34. Newton, G. L., Dorian, R., and Fahey, R. C. (1981) Analysis of biological thiols: derivatization with monobromobimane and separation by reverse-phase high-performance liquid chromatography. *Anal. Biochem.* **114,** 383–387 CrossRef Medline
35. Wintner, E. A., Deckwerth, T. L., Langston, W., Bengtsson, A., Leviten, D., Hill, P., Insko, M. A., Dumpit, R., VandenEkart, E., Toombs, C. F., and Szabo, C. (2010) A monobromobimane-based assay to measure the pharmacokinetic profile of reactive sulphide species in blood. *Br. J. Pharmacol.* **160,** 941–957 CrossRef Medline
36. Ditrói, T., Nagy, A., Martinelli, D., Rosta, A., Kožich, V., and Nagy, P. (2019) Comprehensive analysis of how experimental parameters affect H_2S measurements by the monobromobimane method. *Free Radic. Biol. Med.* **136,** 146–158 CrossRef Medline
37. Portillo-Ledesma, S., Sardi, F., Manta, B., Tourn, M. V., Clippe, A., Knoops, B., Alvarez, B., Coitiño, E. L., and Ferrer-Sueta, G. (2014) Deconstructing the catalytic efficiency of peroxiredoxin-5 peroxidatic cysteine. *Biochemistry* **53,** 6113–6125 CrossRef Medline
38. Hughes, M. N., Centelles, M. N., and Moore, K. P. (2009) Making and working with hydrogen sulfide: The chemistry and generation of hydrogen sulfide in vitro and its measurement in vivo: a review. *Free Radic. Biol. Med.* **47,** 1346–1353 CrossRef Medline
39. Bianco, C. L., Akaike, T., Ida, T., Nagy, P., Bogdandi, V., Toscano, J. P., Kumagai, Y., Henderson, C. F., Goddu, R. N., Lin, J., and Fukuto, J. M. (2019) The reaction of hydrogen sulfide with disulfides: formation of a stable trisulfide and implications for biological systems. *Br. J. Pharmacol.* **176,** 671–683 CrossRef Medline
40. Hoops, S., Sahle, S., Gauges, R., Lee, C., Pahle, J., Simus, N., Singhal, M., Xu, L., Mendes, P., and Kummer, U. (2006) COPASI—a COmplex PAthway SImulator. *Bioinformatics.* **22,** 3067–3074 CrossRef Medline
41. Østergaard, H., Tachibana, C., and Winther, J. R. (2004) Monitoring disulfide bond formation in the eukaryotic cytosol. *J. Cell Biol.* **166,** 337–345 CrossRef Medline
42. Morgan, B., Ezeriņa, D., Amoako, T. N., Riemer, J., Seedorf, M., and Dick, T. P. (2013) Multiple glutathione disulfide removal pathways mediate cytosolic redox homeostasis. *Nat. Chem. Biol.* **9,** 119–125 CrossRef Medline
43. Dóka, É., Pader, I., Bíró, A., Johansson, K., Cheng, Q., Ballagó, K., Prigge, J. R., Pastor-Flores, D., Dick, T. P., Schmidt, E. E., Arnér, E. S. J., and Nagy, P. (2016) A novel persulfide detection method reveals protein persulfide- and polysulfide-reducing functions of thioredoxin and glutathione systems. *Sci. Adv.* **2,** e1500968 CrossRef Medline
44. Zivanovic, J., Kouroussis, E., Kohl, J. B., Adhikari, B., Bursac, B., Schott-Roux, S., Petrovic, D., Miljkovic, J. L., Thomas-Lopez, D., Jung, Y., Miler, M., Mitchell, S., Milosevic, V., Gomes, J. E., Benhar, M., *et al.* (2019) Selective persulfide detection reveals evolutionarily conserved antiaging effects of S-sulfhydration. *Cell Metab.* **30,** 1152–1170.e13 CrossRef Medline
45. Liu, D. K., and Chang, S. G. (1987) Kinetic study of the reaction between cystine and sulfide in alkaline solutions. *Can. J. Chem.* **65,** 770–774 CrossRef
46. Singh, R., and Whitesides, G. M. (1993) Thiol—disulfide interchange. in *Sulphur-Containing Functional Groups* (Patai, S., and Rappoport, Z. eds.), pp. 633–658, John Wiley & Sons, CrossRef
47. Koppenol, W. H., and Bounds, P. L. (2017) Signaling by sulfur-containing molecules. Quantitative aspects. *Arch. Biochem. Biophys.* **617,** 3–8 CrossRef Medline
48. Sardi, F., Manta, B., Portillo-Ledesma, S., Knoops, B., Comini, M. A., and Ferrer-Sueta, G. (2013) Determination of acidity and nucleophilicity in thiols by reaction with monobromobimane and fluorescence detection. *Anal. Biochem.* **435,** 74–82 CrossRef Medline
49. Benson, S. W. (1978) Thermochemistry and kinetics of sulfur-containing molecules and radicals. *Chem. Rev.* **78,** 23–35 CrossRef
50. Bailey, T. S., Zakharov, L. N., and Pluth, M. D. (2014) Understanding hydrogen sulfide storage: probing conditions for sulfide release from hydrodisulfides. *J. Am. Chem. Soc.* **136,** 10573–10576 CrossRef Medline
51. Bailey, T. S., and Pluth, M. D. (2015) Reactions of isolated persulfides provide insights into the interplay between H_2S and persulfide reactivity. *Free Radic. Biol. Med.* **89,** 662–667 CrossRef Medline
52. Kawamura, S., Horii, T., and Tsurugi, J. (1971) Aryl hydrodisulfides. *J. Org. Chem.* **36,** 3677–3680 CrossRef
53. Yu, H.-Z., Yang, Y.-M., Zhang, L., Dang, Z.-M., and Hu, G.-H. (2014) Quantum-chemical predictions of pKa's of thiols in DMSO. *J. Phys. Chem. A.* **118,** 606–622 CrossRef Medline
54. Trujillo, M., and Radi, R. (2002) Peroxynitrite reaction with the reduced and the oxidized forms of lipoic acid: new insights into the reaction of peroxynitrite with thiols. *Arch. Biochem. Biophys.* **397,** 91–98 CrossRef Medline
55. Cuevasanta, E., Zeida, A., Carballal, S., Wedmann, R., Morzan, U. N., Trujillo, M., Radi, R., Estrin, D. A., Filipovic, M. R., and Alvarez, B. (2015) Insights into the mechanism of the reaction between hydrogen sulfide and peroxynitrite. *Free Radic. Biol. Med.* **80,** 93–100 CrossRef Medline
56. Ferrer-Sueta, G., Campolo, N., Trujillo, M., Bartesaghi, S., Carballal, S., Romero, N., Alvarez, B., and Radi, R. (2018) Biochemistry of peroxynitrite and protein tyrosine nitration. *Chem. Rev.* **118,** 1338–1408 CrossRef Medline
57. Trujillo, M., Clippe, A., Manta, B., Ferrer-Sueta, G., Smeets, A., Declercq, J.-P., Knoops, B., and Radi, R. (2007) Pre-steady state kinetic characterization of human peroxiredoxin 5: taking advantage of Trp84 fluorescence increase upon oxidation. *Arch. Biochem. Biophys.* **467,** 95–106 CrossRef Medline
58. Hoffmann, M. R. (1977) Kinetics and mechanism of oxidation of hydrogen sulfide by hydrogen peroxide in acidic solution. *Environ. Sci. Technol.* **11,** 61–66 CrossRef
59. Haynes, W. M. (2014) *CRC Handbook of Chemistry and Physics*, 95th ed, CRC Press, Oakville
60. Zeida, A., Babbush, R., González Lebrero, M. C., Trujillo, M., Radi, R., and Estrin, D. A. (2012) Molecular basis of the mechanism of thiol oxidation by hydrogen peroxide in aqueous solution: challenging the SN2 paradigm. *Chem. Res. Toxicol.* **25,** 741–746 CrossRef Medline
61. Zeida, A., Lebrero, M. C. G., Radi, R., Trujillo, M., and Estrin, D. A. (2013) Mechanism of cysteine oxidation by peroxynitrite: an integrated experimental and theoretical study. *Arch. Biochem. Biophys.* **539,** 81–86 CrossRef Medline
62. Zeida, A., Reyes, A. M., Lebrero, M. C. G., Radi, R., Trujillo, M., and Estrin, D. A. (2014) The extraordinary catalytic ability of peroxiredoxins: a combined experimental and QM/MM study on the fast thiol oxidation step. *Chem. Commun.* **50,** 10070–10073 CrossRef Medline
63. Eyring, H. (1935) The activated complex in chemical reactions. *J. Chem. Phys.* **3,** 107–115 CrossRef
64. Awoonor-Williams, E. and Rowley, C. N. (2018) The hydration structure of methylthiolate from QM/MM molecular dynamics. *J. Chem. Phys.* **149,** 045103 CrossRef Medline
65. Jencks, W. P., and Carriuolo, J. (1960) Reactivity of nucleophilic reagents toward esters. *J. Am. Chem. Soc.* **82,** 1778–1786 CrossRef
66. Ferrer-Sueta, G., Manta, B., Botti, H., Radi, R., Trujillo, M., and Denicola, A. (2011) Factors affecting protein thiol reactivity and specificity in peroxide reduction. *Chem. Res. Toxicol.* **24,** 434–450 CrossRef Medline
67. Fina, N. J., and Edwards, J. O. (1973) The alpha effect. A review. *Int. J. Chem. Kinet.* **5,** 1–26 CrossRef
68. Buncel, E., and Um, I.-H. (2004) The α-effect and its modulation by solvent. *Tetrahedron.* **60,** 7801–7825 CrossRef
69. Trummal, A., Lipping, L., Kaljurand, I., Koppel, I. A., and Leito, I. (2016) Acidity of strong acids in water and dimethyl sulfoxide. *J. Phys. Chem. A.* **120,** 3663–3669 CrossRef Medline
70. Williams, M. (2006) *The Merck Index: An Encyclopedia of Chemicals, Drugs, and Biologicals.* (O'Neil, M. J. ed.) 14th ed., Merck Inc., Whitehouse Station/Rahway, New Jersey CrossRef

71. Silverstein, T. P., and Heller, S. T. (2017) pKa values in the undergraduate curriculum: what is the real pKa of water? *J. Chem. Educ.* **94,** 690–695 CrossRef
72. Landry, A. P., Moon, S., Kim, H., Yadav, P. K., Guha, A., Cho, U.-S., and Banerjee, R. (2019) A catalytic trisulfide in human sulfide quinone oxidoreductase catalyzes coenzyme A persulfide synthesis and inhibits butyrate oxidation. *Cell Chem. Biol.* **26,** 1515–1525.e4 CrossRef Medline
73. Landry, A. P., Moon, S., Bonanata, J., Cho, U. S., Coitiño, E. L., and Banerjee, R. (2020) Dismantling and rebuilding the trisulfide cofactor demonstrates its essential role in human sulfide quinone oxidoreductase. *J. Am. Chem. Soc.* **142,** 14295–14306 CrossRef
74. Kosower, E. M., and Kosower, N. S. (1995) Bromobimane probes for thiols. *Methods Enzymol.* **251,** 133–148 CrossRef Medline
75. Nelson, D. P., and Kiesow, L. A. (1972) Enthalpy of decomposition of hydrogen peroxide by catalase at 25 °C (with molar extinction coefficients of H2O2 solutions in the UV). *Anal. Biochem.* **49,** 474–478 CrossRef Medline
76. Bonanata, J., Turell, L., Antmann, L., Ferrer-Sueta, G., Botasini, S., Méndez, E., Alvarez, B., and Coitiño, E. L. (2017) The thiol of human serum albumin: acidity, microenvironment and mechanistic insights on its oxidation to sulfenic acid. *Free Radic. Biol. Med.* **108,** 952–962 CrossRef Medline
77. Saha, A., Goldstein, S., Cabelli, D., and Czapski, G. (1998) Determination of optimal conditions for synthesis of peroxynitrite by mixing acidified hydrogen peroxide with nitrite. *Free Radic. Biol. Med.* **24,** 653–659 CrossRef Medline
78. Bohle, D. S., Hansert, B., Paulson, S. C., and Smith, B. D. (1994) Biomimetic synthesis of the putative cytotoxin peroxynitrite, ONOO-, and its characterization as a tetramethylammonium salt. *J. Am. Chem. Soc.* **116,** 7423–7424 CrossRef
79. Ellis, K. J., and Morrison, J. F. (1982) Buffers of constant ionic strength for studying pH-dependent processes. *Methods Enzymol.* **87,** 405–426 CrossRef Medline
80. Frisch, M., Trucks, G., Schlegel, H., Scuseria, G., Robb, M., Cheeseman, J., Scalmani, G., Barone, V., Mennucci, B., Petersson, G., *et al.* (2009) *Gaussian 09*. Gaussian Inc., Wallingford, Connecticut
81. Nitsche, M. A., Ferreria, M., Mocskos, E. E., and González Lebrero, M. C. (2014) GPU accelerated implementation of density functional theory for hybrid QM/MM simulations. *J. Chem. Theory Comput.* **10,** 959–967 CrossRef Medline
82. Marcolongo, J. P., Zeida, A., Semelak, J. A., Foglia, N. O., Morzan, U. N., Estrin, D. A., González Lebrero, M. C., and Scherlis, D. A. (2018) Chemical reactivity and spectroscopy explored from QM/MM molecular dynamics simulations using the LIO code. *Front. Chem.* **6,** 70 CrossRef Medline
83. Humphrey, W., Dalke, A., and Schulten, K. (1996) VMD: Visual molecular dynamics. *J. Mol. Graph.* **14,** 33–38 CrossRef Medline
84. Godbout, N., Salahub, D. R., Andzelm, J., and Wimmer, E. (1992) Optimization of Gaussian-type basis sets for local spin density functional calculations. Part I. Boron through neon, optimization technique and validation. *Can. J. Chem.* **70,** 560–571 CrossRef
85. Perdew, J. P., Burke, K., and Ernzerhof, M. (1996) Generalized gradient approximation made simple. *Phys. Rev. Lett.* **77,** 3865–3868 CrossRef Medline
86. Tomasi, J., Mennucci, B., and Cammi, R. (2005) Quantum mechanical continuum solvation models. *Chem. Rev.* **105,** 2999–3094 CrossRef Medline
87. Neves, R. P. P., Fernandes, P. A., Varandas, A. J. C., and Ramos, M. J. (2014) Benchmarking of density functionals for the accurate description of thiol–disulfide exchange. *J. Chem. Theory Comput.* **10,** 4842–4856 CrossRef Medline
88. Chai, J.-D., and Head-Gordon, M. (2008) Long-range corrected hybrid density functionals with damped atom–atom dispersion corrections. *Phys. Chem. Chem. Phys.* **10,** 6615–6620 CrossRef Medline
89. Walker, M., Harvey, A. J., Sen, A., and Dessent, C. E. (2013) Performance of M06, M06-2X, and M06-HF density functionals for conformationally flexible anionic clusters: M06 functionals perform better than B3LYP for a model system with dispersion and ionic hydrogen-bonding interactions. *J. Phys. Chem. A.* **117,** 12590–12600 CrossRef Medline
90. Fukui, K. (1981) The path of chemical reactions - the IRC approach. *Acc. Chem. Res.* **14,** 363–368 CrossRef
91. Jorgensen, W. L., Chandrasekhar, J., Madura, J. D., Impey, R. W., and Klein, M. L. (1983) Comparison of simple potential functions for simulating liquid water. *J. Chem. Phys.* **79,** 926–935 CrossRef
92. Wang, J., Wolf, R. M., Caldwell, J. W., Kollman, P. A., and Case, D. A. (2004) Development and testing of a general amber force field. *J. Comput. Chem.* **25,** 1157–1174 CrossRef Medline
93. Berendsen, H. J. C., Postma, J. P. M., van Gunsteren, W. F., DiNola, A., and Haak, J. R. (1984) Molecular dynamics with coupling to an external bath. *J. Chem. Phys.* **81,** 3684–3690 CrossRef
94. Torrie, G. M., and Valleau, J. P. (1977) Nonphysical sampling distributions in Monte Carlo free-energy estimation: umbrella sampling. *J. Comput. Phys.* **23,** 187–199 CrossRef
95. Kästner, J. (2011) Umbrella sampling. *WIREs Comput. Mol. Sci.* **1,** 932–942 CrossRef
96. Semelak, J. A., Battistini, F., Radi, R., Trujillo, M., Zeida, A., and Estrin, D. A. (2019) Multi-scale modeling of thiol overoxidation in peroxiredoxins by hydrogen peroxide. *J. Chem. Inf. Model.* CrossRef Medline
97. Schneider, T., and Stoll, E. (1978) Molecular-dynamics study of a three-dimensional one-component model for distortive phase transitions. *Phys. Rev. B.* **17,** 1302–1322 CrossRef
98. Kästner, J., and Thiel, W. (2005) Bridging the gap between thermodynamic integration and umbrella sampling provides a novel analysis method: "Umbrella integration". *J. Chem. Phys.* **123,** 144104 CrossRef Medline
99. Gerasimov, O. V., and Lymar, S. V. (1999) The yield of hydroxyl radical from the decomposition of peroxynitrous acid. *Inorg. Chem.* **38,** 4317–4321 CrossRef
100. Declercq, J. P., Evrard, C., Clippe, A., Stricht, D. V., Bernard, A., and Knoops, B. (2001) Crystal structure of human peroxiredoxin 5, a novel type of mammalian peroxiredoxin at 1.5 Å resolution. *J. Mol. Biol.* **311,** 751–759 CrossRef Medline